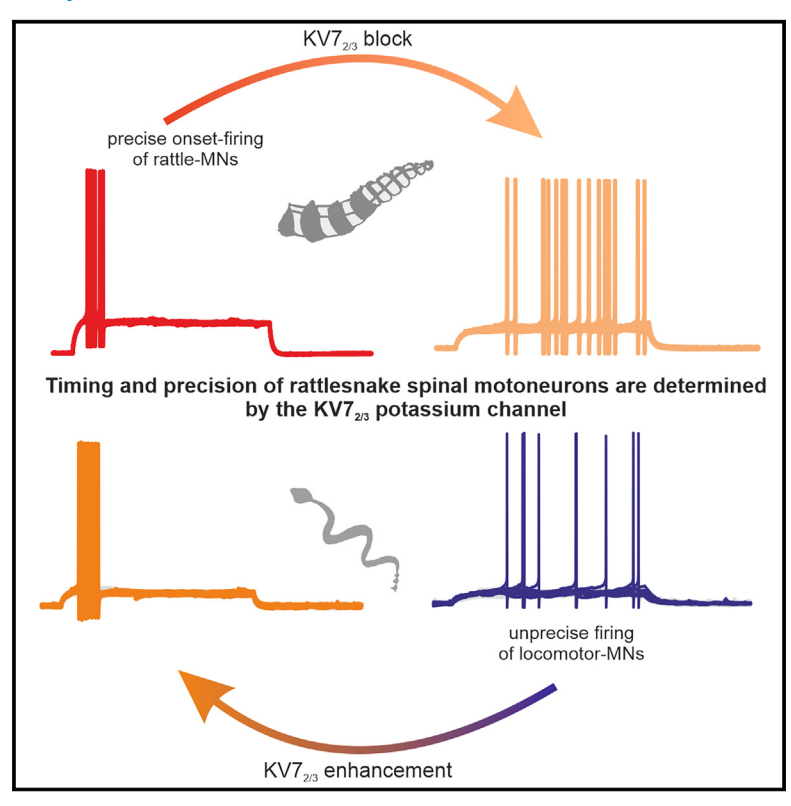
Timing and precision of rattlesnake spinal motoneurons are determined by the KV7_{2/3} potassium channel

Graphical abstract



Authors

Maximilian S. Bothe, Tobias Kohl, Felix Felmy, Jason Gallant, Boris P. Chagnaud

Correspondence

maximilian.bothe@uni-graz.at

In brief

Bothe et al. show how motoneurons in the spinal cord of rattlesnakes are tuned to transmit CPG activity that controls motion in widely different time domains for locomotion and rattling, respectively. Their underlying physiological differences are largely based on KV7_{2/3} channels, which affect the timing and precision of motoneuronal activity.

Highlights

- Rattlesnake motoneurons are tuned to different behaviors
- Timing and precision of motoneuron firing are determined by KV7_{2/3} channels
- Motoneuron activity is not based on differential expression of KV7_{2/3} transcripts





Article

Timing and precision of rattlesnake spinal motoneurons are determined by the KV7_{2/3} potassium channel

Maximilian S. Bothe, 1,6,* Tobias Kohl, 2 Felix Felmy, 3 Jason Gallant, 4 and Boris P. Chagnaud 1,5

*Correspondence: maximilian.bothe@uni-graz.at https://doi.org/10.1016/j.cub.2023.11.062

SUMMARY

The evolution of novel motor behaviors requires modifications in the central pattern generators (CPGs) controlling muscle activity. How such changes gradually lead to novel behaviors remains enigmatic due to the long time course of evolution. Rattlesnakes provide a unique opportunity to investigate how a locomotor CPG was evolutionarily modified to generate a novel behavior—in this case, acoustic signaling. We show that motoneurons (MNs) in the body and tail spinal cord of rattlesnakes possess fundamentally different physiological characteristics, which allow MNs in the tail to integrate and transmit CPG output for controlling superfast muscles with high temporal precision. Using patch-clamp electrophysiology, we demonstrate that these differences in locomotor and rattle MNs are mainly determined by KV7_{2/3} potassium channels. However, although KV7_{2/3} exerted a significantly different influence on locomotor and rattle MN physiology, single-cell RNA-seq unexpectedly did not reveal any differences in KV7_{2/3} channels' expression.

INTRODUCTION

Vertebrate locomotor behavior is governed by neuronal networks located in the hindbrain and spinal cord, which control the activation sequences of muscle contractions. These central pattern generators (CPGs) elicit different types of behaviors, such as swimming, ¹⁻⁷ flying, ^{8,9} or bi- and quadrupedal locomotion.^{5,8-11} Across species, locomotor patterns show vastly different frequency and precision regimes: while orcas use fin movements around two hertz (Hz), 12 Xenopus tadpoles produce faster body undulation around 20 Hz.¹³ Such variable motor control is also found in flying and terrestrial locomotion: hummingbirds show wingbeat frequencies between 40 and 60 Hz, 14-16 whereas gulls beat their wings around 3 Hz, 17 cheetahs run at stride speeds of 4 Hz, 18 while sloths locomote at frequencies of up to 0.75 Hz.¹⁹ Despite the variability of locomotor patterns, the basic blueprint of spinal CPGs consists of conserved building blocks. 5,20,21 These are formed by (1) groups of interneurons that regulate ipsi- and contralateral activities and (2) the motoneurons (MNs), which convey CPG output to the muscles and can also contribute to rhythm generation.^{5,21-23} How CPGs are tuned to different motion regimes, especially to frequency and precision in different species, however, still remains enigmatic.

Within a motor circuit, the intrinsic properties and connectivity of interneurons determine the frequency and pattern(s) of muscle activation.^{24,25} To transmit CPG activity to the muscles without

major deformation of timing and pattern, MNs need to fire in the respective time domains. Consequentially, MN intrinsic properties differ, depending on the behavior they are associated with, as shown for different pools of premotor and MNs in zebrafish. ^{6,22,26–30} The underlying physiological basis of such differences in spinal MNs, besides soma size, ^{31,32} depends on differences in ion-channel composition and expression, but comparative studies remain scarce. As precisely timed transmission of CPG output becomes increasingly important with higher repetition rates of a given motor behavior, fast locomotor rhythms rely heavily on the precise activation and deactivation of associated MN pools.

One major problem in comparing spinal CPGs across locomotor behaviors is interspecies comparability: the small but manyfold shifts in CPG architecture and physiology that occurred during the evolution of different species mask essential adaptations in network constituents that provided the initial basis for a change in motor behavior. Rattlesnakes provide a unique opportunity to overcome this hurdle: they possess differently adapted spinal CPGs that work in different frequency and precision regimes: a slow CPG for locomotor behavior (e.g., undulation at 1–2 Hz), working in a similar frequency regime as those of other snakes, ^{33–36} and a fast CPG for acoustic communication (rattling around 100 Hz^{37,38}).

We investigated the adaptations that enable the vast difference in frequency and precision regimes of rattlesnake MN activity that controls locomotion and rattling. Due to the importance of MNs in the execution of motor behaviors, we focused on the

¹Institute of Biology, University of Graz, 8010 Graz, Austria

²TUM School of Life Science, Technical University of Munich, 85354 Munich, Germany

³Institute of Zoology, University of Veterinary Medicine Hannover, 30559 Hannover, Germany

⁴Department of Integrative Biology, Michigan State University, East Lansing, MI 48824, USA

⁵Department of Biology II, Ludwig-Maximilians-University Munich, 82152 Planegg-Martinsried, Germany

⁶Lead contact



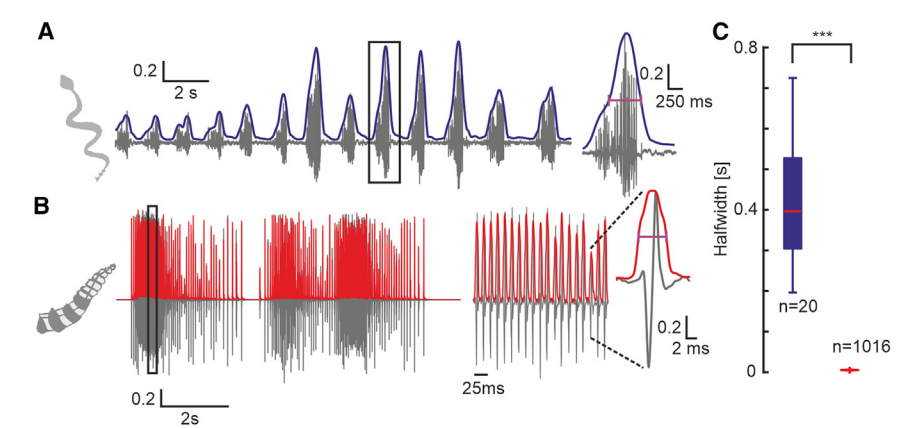


Figure 1. EMG recordings of rattlesnake torso (blue) and rattle (red) muscle

(A and B) Example EMG recordings (gray) and root-mean-square envelopes (color) from locomotor (A) and rattle (B) muscles during free moving behavior. Black boxes indicate zoom in regions plotted on smaller time scales.

(C) The half-width of individual events was significantly different between locomotion and rattling $(p = 1.76 \times 10^{-14}, Mann-Whitney U test)$. In boxplots, the central marker (line) indicates the median value, and the bottom and top edges of the box show the 25th and 75th percentiles, respectively.

properties that allow MNs to perform as efficient senders of highfrequency, precise, and ongoing network output. While the faster rhythm of the rattle CPG is likely due to adaptations at the interneuron level, we show that the precise transmission of CPG activity to the rattle muscles depends on the intrinsic membrane properties of spinal MNs. Pharmacologically modifying the activity of the non-inactivating KV72/3 channel was sufficient to impose locomotor-like activity onto rattle MNs and vice versa. Interestingly, single-cell RNA-seq did not reveal any significant differences in the channels' expression profile between locomotor and rattle MNs. Our data thus suggest that changes in posttranslational modifications contribute to the different effects of KV7_{2/3} channels. We propose that such changes in MN physiology contribute to the evolution of different motor behaviors across vertebrates.

RESULTS

Neuromuscular activity of locomotor and rattling behavior

Electromyography (EMG) recordings of muscles involved in locomotion or rattling displayed distinct activity patterns (Figure 1). In line with the different modes of rattlesnake locomotor behavior (undulatory, caterpillar, and concertina^{34,36}), left-right alternating patterns, and rhythmic simultaneous activation of both cord sides occurred in the locomotor region. Individual bouts of locomotor activity on each side of the animal displayed activations of hundreds of milliseconds in duration (Figure 1A). Envelopes of individual bouts (Figure 1A, blue) displayed half-widths of 425 \pm 34.8 ms (Figure 1C, blue, n = 20 events). The length of muscle activity was therefore in the same time domain as in EMGs previously recorded in other snakes³³⁻³⁶ and vertebrates.³⁹⁻⁴³

EMG activity in the rattle muscles showed distinct left-right alternating activation patterns, as described in previous reports. 44,45 In contrast to locomotor EMG bouts, rattle activity was characterized by very short activations (Figure 1B) with half-widths of individual envelopes of 5.4 ± 0.02 ms (Figure 1C, red, n = 1,016 events). These individual peaks reflected the synchronous activation of MNs and muscle fibers needed to reach fast contraction frequencies. Thus, the two cord regions show distinct profiles in left-right alternating activity and precision.

MNs in both cord regions thus need to work in vastly different time regimes to efficiently integrate and transmit CPG network activity to the muscles to control locomotion and rattling.

Rattle and locomotor MNs differ in biophysical membrane properties

Next, we asked which physiological adaptations lead to the differences in locomotor and rattle EMGs. As MNs govern this activity by transmitting CPG-generated locomotor rhythms, we performed whole-cell patch-clamp recordings from MNs in spinal cord slices from the locomotor and rattle regions (Figure 2). Despite their shared spinal origin, rattle (MN-R) and locomotor (MN-L) MNs displayed significantly different basal membrane properties (Figures 2A-2D), action potential (AP) parameters (Figures 2E-2H), and rheobase currents (Figure 2I). Input resistance (Figure 2B) and membrane time constant (Tau, Figure 2C) were significantly larger in MN-L than in MN-R (R_{in}-L: 423.24 ± 46.33 MΩ, n = 12, R_{in} -R: 119.83 ± 11.39 MΩ, n = 32, p = 2.536×10^{-9} : Tau-L: 36.46 ± 3.13 ms. n = 12. Tau-R: 7.97 ± 0.94 ms, n = 32, p = 1.833×10^{-9}). The resting membrane potential (RMP) was more negative in MN-R compared with MN-L (Figure 2D, RMP-L: -64.34 ± 0.9 mV, n = 22, RMP-R: -67.56 ± 0.8 mV, n = 32, p = 0.0226). As expected from their membrane properties, the rheobase was significantly higher in MN-R compared with MN-L (Figure 2I; Rheo-L: $31.96 \pm 4.7 \text{ pA}, \text{ n} = 22, \text{Rheo-R: } 180.03 \pm 15.9 \text{ pA}, \text{ n} = 32,$ $p = 5.333 \times 10^{-9}$). The full width at half-maximum of AP and AHP (afterhyperpolarization) also displayed significant differences, the amplitude of the APs was, however, not different (Figures 2F–2H, AP_{EWHM} -L: 0.49 ± 0.016 ms, n = 22, AP_{EWHM} -R: 0.32 ± 0.011 ms, n = 32, p = 1.248×10^{-8} ; AHP_{FWHM}-L: 2.91 ± $0.606 \text{ ms}, n = 22, AHP_{FWHM}-R: 1.06 \pm 0.156 \text{ ms}, n = 32, p =$ 1.004×10^{-7} ; AP_{Amp}-L: 97.3 ± 5.63 mV, n = 22, AP_{Amp}-S: 99.18 ± 7.63 mV, n = 32, p = 0.142). When probing the currentfrequency curves (I-F curves) of MNs by stepwise incrementing current amplitudes (Figures 2J and 2K), MN-R started firing at higher currents and also displayed higher maximum frequencies (Figures 2L and 2M; f_{max} -L = 110.00 ± 4.89 Hz, n = 22, f_{max} -R = $194.02 \pm 8.92 \text{ Hz}$, n = 32, p = 1.792×10^{-7}). The AP voltage threshold, however, was similar in both MN types (Figure 2N, $V_{thres.}$ -L: -38.69 ± 0.98 mV, n = 22, $V_{thres.}$ -R: $-39.44 \pm$ 1.21 mV, n = 32, p = 0.7314).

Current Biology Article



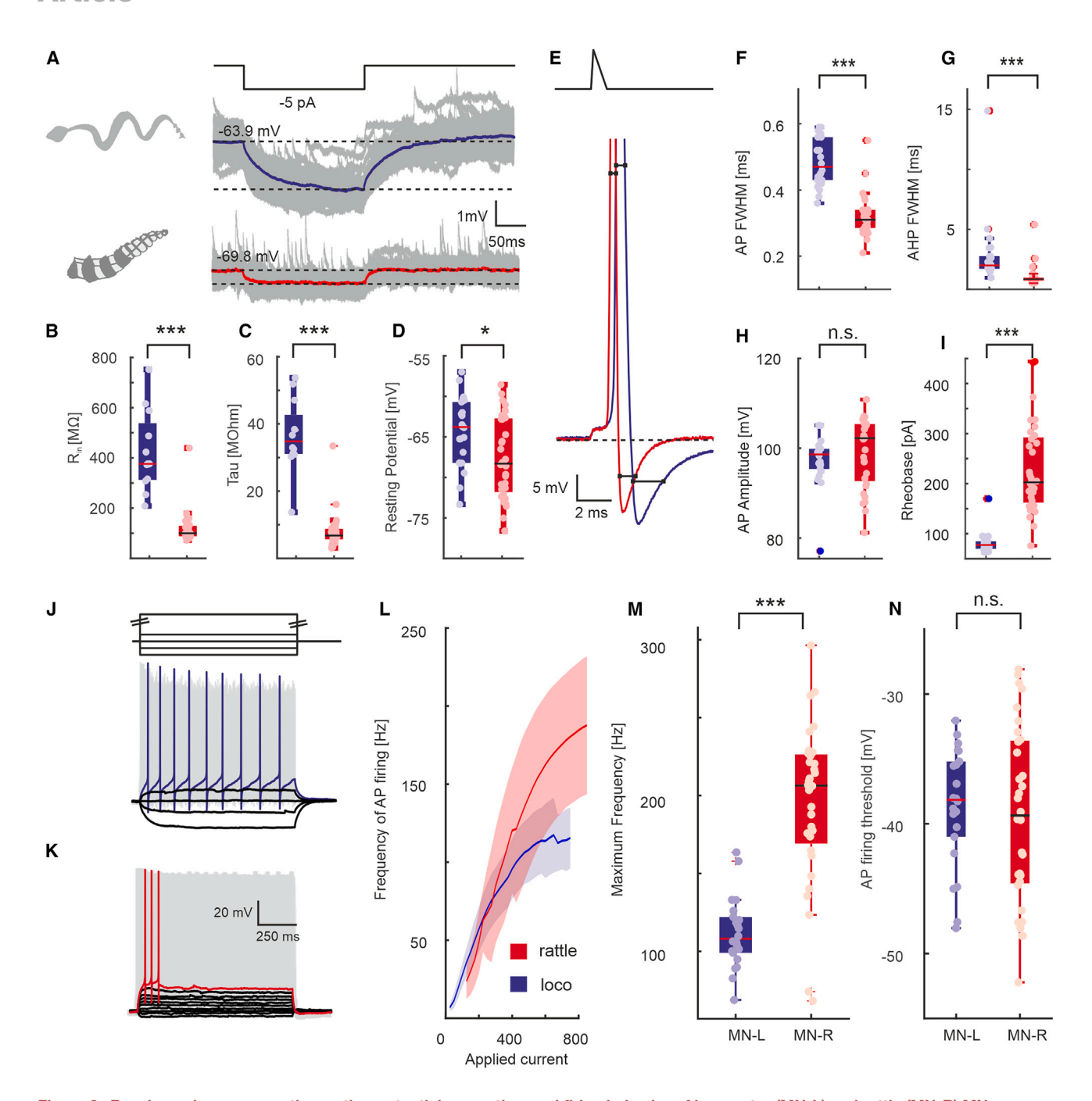


Figure 2. Basal membrane properties, action potential properties, and firing behavior of locomotor (MN-L) and rattle (MN-R) MNs (A-D) Recordings of a MN-L (middle, blue) and MN-R (bottom, red) stimulated with current steps (top, black) (A). MN-L showed significantly higher input re-

sistances (B), Tau values (C), and resting membrane potentials (D). (E-H) (E) Single action potentials (APs) recorded from MN-L (bottom, blue) and MN-R (bottom, red) stimulated with short ramp stimuli (top). MN-L displayed

significantly wider full width at half-maximum (FWHM) for AP (F) and after hyperpolarization (AHP) (G). AP height did not differ significantly (H).

(I) MN-L displayed significantly lower rheobase values. MN-L (J) and MN-R (K) stimulated with incrementally rising current steps. MN-L (blue) started firing at lower input currents (L, plot shows mean frequencies ± SD) and reached significantly lower maximum firing frequencies (M) than MN-R.

(N) MN-L and MN-R revealed similar firing thresholds. Statistics: Mann-Whitney U test. p values: *** < 0.001, * < 0.05; n.s., non-significant. In boxplots, the central marker (line) indicates the median value, and the bottom and top edges of the box show the 25th and 75th percentiles, respectively.

In vitro backfills of rattle and locomotor spinal nerves

Cell size is a determining factor of membrane properties and neuronal activation. 31,32 Therefore, we investigated whether a difference in soma size contributed to the different membrane properties of MN-R and MN-L by backfilling MNs via ventral roots (Figures 3A and 3B, white arrowheads). No significant difference



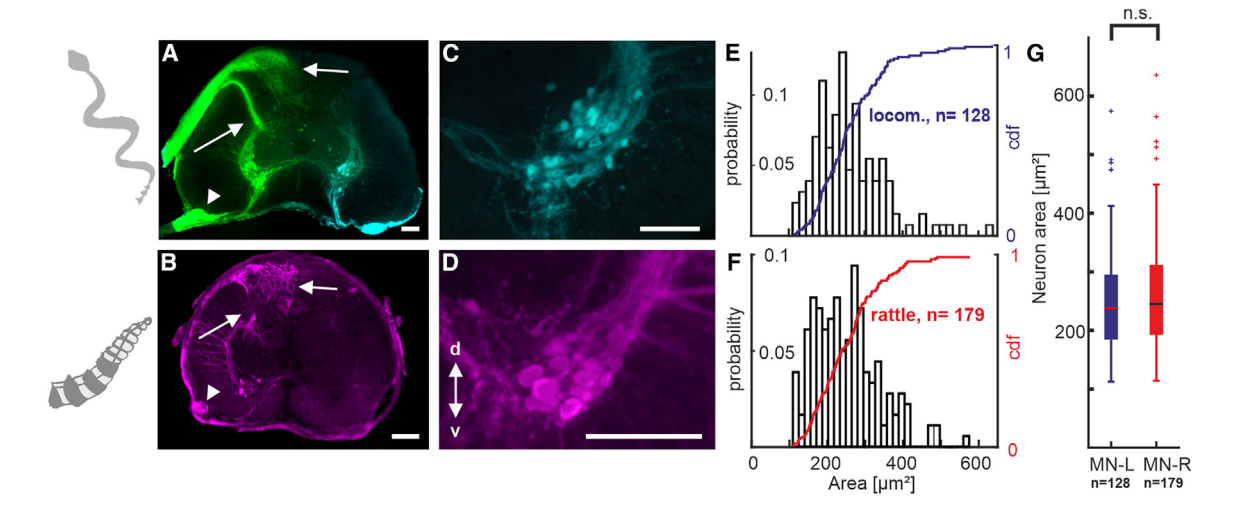


Figure 3. Spinal nerve backfills in segments from torso (green, cyan) and tail (magenta) spinal cord (A-D) Bilateral backfills of ventral roots (arrowheads) in locomotor spinal cord (A), and unilateral backfill in rattle spinal cord (B). Dorsal roots innervated the dorsal part of the cord and the dendritic fields of MNs (white arrows). Magnified view of MN-L (C) and MN-R (D) stained in a different set of experiments. (E and F) Histogram and cumulative distribution function (cdf) of individual MN soma areas from locomotor (E) and rattle (F) spinal cord. (G) Differences between the areas of individual MN-L and MN-R were non-significant. Abbreviations are as follows: d, dorsal; v, ventral. Scale bars, 100 µm. Statistics: Mann-Whitney U test. n.s., non-significant. In boxplots, the central marker (line) indicates the median value, and the bottom and top edges of the box show the 25th and 75th percentiles, respectively. For an overview of ventral and dorsal root projections in rattlesnake spinal cord see Figure S1.

was observed in the MN soma sizes between both parts of the cord (Figures 3E-3G, MN-L: 260.90 \pm 8.11 μ m², n = 128; MN-R: $251.18 \pm 6.38 \ \mu m^2, \ n$ = 179; p = 0.4305), thus ruling out size as a determining factor for the differences in membrane properties.

Rattle MNs fire more precise than locomotor ones

Rattle MNs need to fire simultaneously to generate short and precise motor events (see EMG results). We next tested their spiking reliability at rheobase (Figure 4). MN-R displayed a fast, sub-threshold rectification at stimulus onset (Figure 4B, inset), absent in MN-L (Figure 4A, inset), which became evident in sub-threshold events (Figures 4A and 4B bottom and 4E; onset integral-L: $-74.34 \pm 7.26 \times 10^{-5}$ s V, n = 22, onset integral-R: $15.53 \pm 4.46 \times 10^{-5}$ s V, n = 32, p = 5.35×10^{-9}). The rectifying component promoted strong onset properties (i.e., short first-AP latencies, Figures 4B top and 4C red) and small standard deviation (i.e., "jitter," Figure 4D). MN-L did not show such a rectification. Instead, they steadily approached their new equilibrium potential (Figure 4A, bottom). Accordingly, they revealed much longer first AP (F-AP) latencies (Figures 4A top and 4C blue; F-AP-latency-L: 512.77 ± 29.95 ms, n = 22, F-APlatency-R: 123.23 ± 22.73 ms, n = 32, p = 1.233×10^{-8}) with larger standard deviation (i.e., broader jitter, Figure 4A top and 4D; Jitter-L: 168.42 ± 12.86 ms, n = 22, Jitter-R: 47.24 ± 12.86 12.88 ms, n = 32, p = 5.351×10^{-9}).

Due to the rectifying nature of the onset component in MN-R, we hypothesized that differences in potassium channel expression could explain the electrophysiological properties of MN-L and MN-R. To identify these potassium channels and their contribution, we applied pharmacological treatment to manipulate potassium conductance (Figures 5, 7, S2-S4, and S7).

We first tested the low voltage-activated potassium channel KV1₁.46-49 Blocking KV1₁ current by application of 100 nM α-dendrotoxin partially reduced the fast-rectifying component of sub-threshold current in MN-R (Figure S2; onset integral-R: 24.16 \pm 3.68 \times 10⁻⁵ s V, onset integral-R_{DTx}: 7.81 \pm 2.71 \times 10^{-5} s V, n = 6, p = 0.031) but did not affect the onset firing pattern (Figure S2). This indicated that KV1₁, although present, plays only a minor role in the precise and phasic firing of MN-R. Despite a small and expected shift toward lower rheobase values, accompanied by a lower AP-firing threshold, we also did not find any other effect on active or basal membrane properties (Figure S3).

Next, we investigated the contribution of the non-inactivating KV7_{2/3} channels, which are known to modulate MN excitability in the spinal cord. $^{50-52}$ Application of the KV7 $_{2/3}$ blocker XE991, completely abolished the phasic properties of MN-R (Figures 5A and 5B). This was accompanied by a significant increase in their input resistance (Figure S4B, Rin-R: 120.96 ± 13.76 M Ω , n = 8, R_{in}- R_{XE991}: 158.19 \pm 19.33 M Ω , n = 8, p = 0.0078). After XE991 treatment, MN-R displayed significantly longer first spike latencies (Figure 5C, F-AP-latency-R: 98.22 ± 9.93 ms, F-AP-latency- R_{XE991} : 332.93 ± 39.85 ms, n = 8, p = 0.008), jitter (Figure 5D, jitter-R: 25.40 \pm 3.95 ms, jitter-R_{XE991}: 157.68 ± 28.98 ms, n = 8, p = 0.008), and a reduction in the onset repolarizing component (Figure 5A, 5B bottom, 5E, onset integral-R: $8.5 \pm 5.94 \times 10^{-5}$ s V, onset integral-R_{XE991}: $-33.84 \pm$ 7.56×10^{-5} s V, n = 8, p = 0.008). While showing a strong trend toward lower values, rheobase of MN-R was not significantly lowered by XE991 application (Figure S4I, Rheo-R: 123.25 ± 22.05 pA, Rheo- R_{XE991} : 95.75 ± 22.92 pA, n = 8, p = 0.0547) and remained above rheobase values of MN-L (see Figure 2I, blue, $p = 6.65 \times 10^{-4}$), indicating that their higher leakiness involved additional ion channels.

Ion-channel expression of locomotor and rattle MNs

We next evaluated the amount of differential expression of KCNQ2 (KV72), KCNQ3 (KV73), and genes coding for other

Current Biology Article



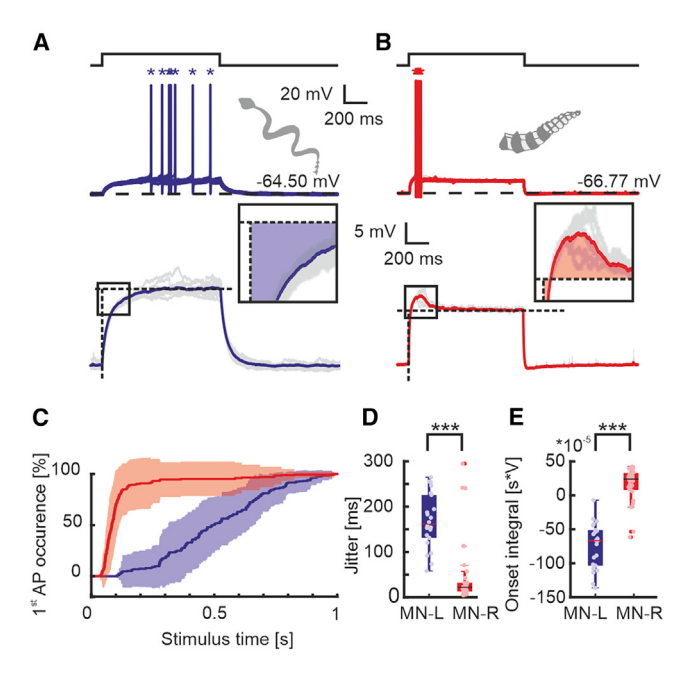


Figure 4. AP latency and jitter of MN-L and MN-R firing

(A and B) Recordings of MN-L (A) and MN-R (B) upon stimulation rheobase current. Recordings grouped into firing (top) and non-firing (bottom) repetitions. MN-R but not MN-L showed a strong, fast repolarizing current after stimulus onset (A, B, bottom traces and insets).

(C) First AP occurrences upon stimulation of MN-L (blue) and MN-R (red). First APs (* in A and B) occurred over a broad range during stimulation in MN-L, while MN-R APs occurred at stimulus onset.

(D and E) The repolarizing onset current mediated smaller jitter (D, measured as SD of first spike occurrences) and stronger onset properties (E) to MN-R firing. Statistics: Mann-Whitney-U-test. p values: *** < 0.001. In boxplots, the central marker (line) indicates the median value, and the bottom and top edges of the box show the 25th and 75th percentiles, respectively.

potassium channels and their auxiliary subunits, which might underlie the different biophysical properties of MN-L and MN-R. We initially performed bulk RNA-seq of locomotor and rattle spinal segments of three rattlesnakes (Figures S5A and S5B). Although differential expression was present in a subset of transcripts, including the well-known developmental genes HOXA11 and HOXB13 (Table S1), bulk sequencing did not reveal significant differences in the expression of any potassium channels or auxiliary subunits to which the different electrophysiological properties of MN-L and MN-R could be attributed (Table S1; Figures S5C-S5E).

We therefore reexamined a set of genes associated with KV channels, using more sensitive reverse-transcription quantitative PCR (RT-qPCR; Figure S6; Tables S2-S4). RNA was extracted from the whole lysate of locomotor and rattle spinal segments (n = 8). Of the investigated KV channels, only KCNQ3 (KV7₃) showed a significantly higher expression (Figure S6A; Table S2#05, p = 0.017) in the rattle spinal cord. All other KV channel transcripts, including KCNC1 (KV3₁), KCNQ2 (KV7₂), and KCNA1 (KV1₁) displayed similar expression in locomotor and rattle spinal cord segments (Figures S6B-S6D; Table S2). We also found that the developmental gene HOXD9 is significantly more strongly expressed in the tissue of the adult rattle spinal cord (Table S2#6, p < 0.001), confirming the caudal origin of the investigated rattle tissue.

Single-cell sequencing

The bulk-sequencing approach of entire cord regions can mask differences in expression at the MN level, due to the tissue included that is not of MN origin. To specify mRNA origin, we performed single-cell sequencing (Figure 6) on 34 locomotor and 41 rattle MNs. As expected from their common motoneuronal origin, MNs from both cord regions showed overlapping RNA expression profiles (Figure 6A). The differential expression analysis revealed 26 differentially expressed (DE) genes of which 23 were identifiable against the tiger rattlesnake genome (Table S5). The choline acetyltransferase (CHAT) gene was used as a control for the MN origin of the data and showed equally high expression in both datasets (Figure 6B). HOXD9 showed significantly higher expression in MN-R (Figure 6C). None of the DE genes were associated with a family of KV channels (Table S5). In particular, KCNQ2 and KCNQ3 showed no significant differences between MN-L and MN-R (Figures 6D and 6E). However, transcripts coding for the ABCC9 (ATP-binding cassette subfamily C member 9, Figure 6F; Table S5#11) protein, a subunit of K_{ATP} channels also referred to as SUR2, showed higher expression in MN-R. Other potentially relevant protein transcripts that showed a significantly higher expression in MN-L included PDE7A (phosphodiesterase 7A, Figure 6G; Table S5#02), LPAR6 (lysophosphatidic acid receptor 6, Table S5#03), and PTPRM (protein tyrosine phosphatase receptor type M, Table S5#14), which all have been described as important components of second-messenger pathways controlling intracellular cAMP levels and protein phosphorylation. Interestingly, we also found the voltage-gated sodium leak channel NALCN to be higher expressed in MN-L (Figure 6H; Table S5#18).

KV7 channels in locomotor MNs

Although we found no differences in the expression of KV7_{2/3} between the two cord regions at the single MN level, our XE991 pharmacology (Figure 5) clearly demonstrated a determining role of these channels in the physiological differences of MN-L and MN-R. We therefore tested whether functional KV7_{2/3} channels were present in MN-L. We bath-applied the specific KV7_{2/3} channel enhancer retigabine while recording from MN-L. After washing in 10 μM retigabine to enhance KV7_{2/3} conductance (Figure 7), MN-L displayed significantly less jitter (Figure 7D, jitter-L: 195.06 ± 23.17 ms, jitter-L_{Retigabine}: 62.11 ± 17.52 ms, n = 8, p = 0.008), shorter onset latencies (Figure 7C, F-AP-latency-L: $528.35 \pm 47.04 \text{ ms F-AP-latency-L}_{Retigabine}$: 200.27 ± 44.92 ms, n = 8, p = 0.008), and higher rheobase values (Figure S7I, Rheo-L: 21.5 ± 1.88 pA, Rheo-L_{Retigabine}: 63.88 ± 11.93 pA, n = 8, p = 0.008), all of which led to phasic firing. Interestingly, MN-L also showed a repolarizing component upon stimulus onset, similar to MN-R under untreated conditions (Figures 7A and 7B bottom, 7E; onset integral-L: $-76.71 \pm 11.64 \times 10^{-5}$ s V, onset integral- $L_{Retigabine}$: 0.56 ± 10.04 × 10⁻⁵ s V, n = 8, p = 0.008). Given that retigabine exerts its impact on the "M-current" by left-shifting its I-V relationship,⁵³ these changes further emphasize the role of KV7_{2/3} channels in decreased tonic excitability and increased spiking precision. Retigabine also affected the input resistance (Figure S7B) and the time constant (Figure S7C), which caused a strong increase in the rheobase of MN-L (Figure S7I), tuning them toward a rattle-like physiology (Figures 7 and S7). Retigabine had no effect on single AP properties (Figures S7E-S7H). Thus, MN-L possesses KV7_{2/3} channels, which can impose MN-R



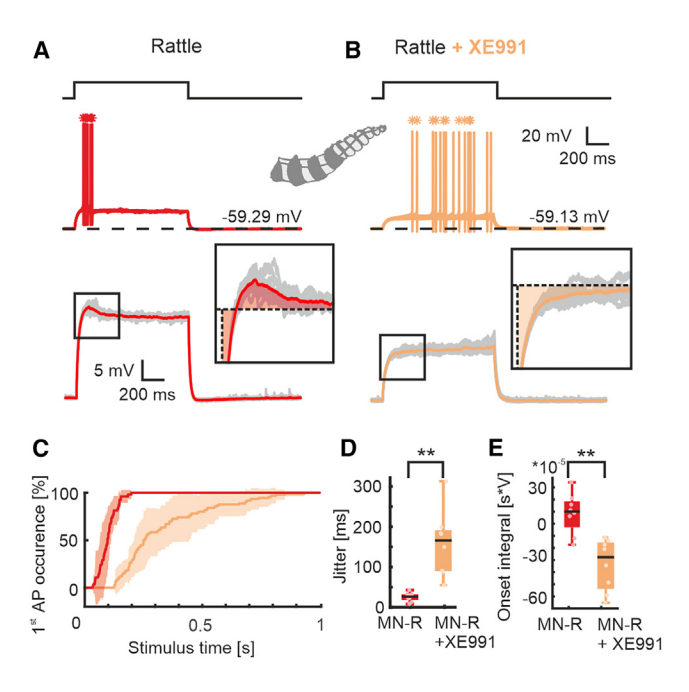


Figure 5. KV7_{2/3} channels mediate the onset properties of rattle motoneurons

(A and B) Traces of an MN-R upon stimulation at rheobase current grouped into firing (top) and non-firing (bottom) repetitions before (A) and after (B) application of XE991. Note the differences in the course of onset voltages (bottom traces and insets). Under XE991 treatment, first APs (* in A and B) occurred in a much broader time window during stimulation with rheobase current.

(C-E) Under XE991 treatment, MN-R onset latency (C) and first AP jitter (D) were significantly increased. Integrals between recording traces and equilibrium potentials after stimulus onset (dashed horizontal line in insets) significantly decreased (E). Statistics: Wilcoxon signed-rank test. p values: ** < 0.01. In boxplots, the central marker (line) indicates the median value, and the bottom and top edges of the box show the 25th and 75th percentiles, respectively. For additional data on XE991 modulation of MN membrane properties and effects of DTx, see Figures S2-S4.

characteristics on them when their voltage activation is shifted to more negative membrane potentials, resulting in a rattle-like pattern for MN-L firing.

DISCUSSION

Neural circuits are sets of neurons defined by their intrinsic membrane properties and their functional connectivity. To generate different behaviors, these circuits need to be adapted. Our anatomical data do not indicate major changes in the organization of MNs controlling locomotion and rattling, respectively. This is not surprising, given that the difference in MN activation frequency for locomotion and rattling likely results from yet uninvestigated adaptations at the interneuron level.

Irrespective of network modifications, MNs need to be physiologically adapted to follow the interneuron activation patterns and, in the case of MN-Rs, sustain high frequency and precise firing for extended periods of time. We show that the intrinsic membrane properties of spinal MNs in the rattlesnake are differently adapted to their tasks. MNs in the locomotor region integrate inputs over time and thus allow for long-lasting muscle contractions, whereas MNs in the rattle region are tuned toward short-latency and precision firing, which benefit the transmission of fast and precise CPG activity to the rattlesnakes' specialized muscles.54,55

KV7_{2/3} channels determine differences in MN physiology

Although their voltage threshold for AP firing is similar, MNs that control the muscles for locomotion and rattling display fundamentally different physiological features, one being the highly phasic activity of MN-R. Our pharmacological treatments show that this difference is mainly based on KV7_{2/3} channels. These channels mediate a slowly activating, non-inactivating potassium current, called the M-current. 56,57 M-currents are of major importance to regulate neural activity by increasing or decreasing the excitability of neurons within networks such as the hippocampus⁵⁸⁻⁶⁰ or the spinal cord, where they influence gait frequency control.⁵¹ Although our data show that KV7_{2/3} mediates the differences in firing behavior reported here, the presence of equal amounts of KV72 and KV73 channel transcripts in single-cell sequencing of MN-L and MN-R raises the question how KV7_{2/3} channels, or their functionality, are altered between the two cord regions.

Several factors are known to modify KV7_{2/3} channels, which could explain the observed differences: KV72/3 channels are formed by tetramers that assemble in variable stoichiometry.⁶¹ The stoichiometry has a major impact on the currents that can be recorded. 62,63 It is however still debated whether such differences are based on membrane trafficking or the functionality of membrane-incorporated channels of different stoichiometries. 62,64-66 Our MN single-cell sequencing did not show differences in the expression of KV72 and KV73 subunits, making a difference in stoichiometry unlikely. The slightly higher abundance of KCNQ3-RNA in rattle spinal cord found in our bulk qPCR, thus likely resulted from a differential expression in other cell types.

Phosphorylation of $\mbox{KV7}_{\mbox{\scriptsize 2/3}}$ channels greatly affects cellular M-currents by increasing or decreasing KV7_{2/3} channel activity. 67-73 One factor that increases KV7_{2/3} currents is an elevated intracellular cAMP level. cAMP influence on KV7_{2/3} channels is due to cAMP-PKA-mediated phosphorylation. ^{67–69} An enhancing effect of [cAMP]_i might thus play a role in the increased KV7_{2/3} currents in MN-R. In our single-cell sequencing, MN-L shows much higher expression levels of RNA coding for phosphodiesterase 7A (PDE7A). PDE7A is a cAMP-specific enzyme that binds with very high affinity and hydrolyzes cAMP.⁷⁴ It can therefore prevent cAMP-PKA-mediated phosphorylation of $KV7_{2/3}$ channels in MN-L. Given the low expression of PDE7A-RNA in MN-R and the presumably also lower abundance of the associated protein, cAMP hydrolysis might be reduced in MN-R, therefore allowing cAMP-PKA-mediated phosphorylation of KV72/3 channels to increase the M-current in these neurons. Thus, differential expression of PDE7A could contribute to the different physiology of MN-L and MN-R.

Potential sub-threshold interplay of NALCN sodium with KV7_{2/3} and K_{ATP} potassium currents

Besides modulations of KV7_{2/3} channel activation and kinetics by posttranslational phosphorylation, its interplay with other

Current Biology Article



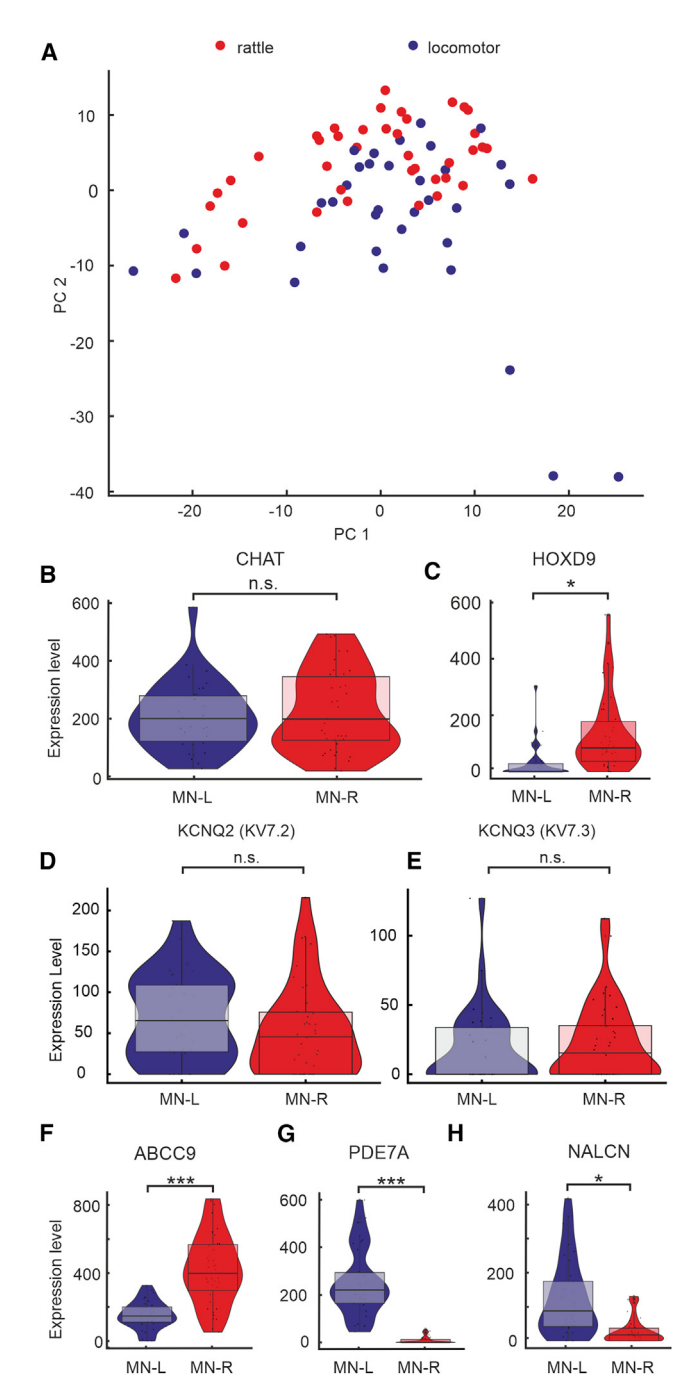


Figure 6. Single-cell RNA-seq of rattlesnake locomotor and rattle MNs

(A) A principal component analysis of the UMI-counts from MN-L and MN-R.As expected, due to their MN origin, data occupy a similar feature space.(B) CHAT was used as a control gene to verify MN origin of the data and was equally high expressed in the MN-L and MN-R datasets.

(C) HOXD9 was significantly higher expressed in MN-R.

(D and E) KCNQ2 (KV7₂) and KCNQ3 (KV7₃) did not show differential expression between MN-L and MN-R.

(F) The K_{ATP} subunit ABCC9 was significantly higher expressed in MN-R. (G and H) Phosphodiesterase 7A (G) and the sodium leak channel NALCN (H) showed significantly higher expression in MN-L. p values: *** < 0.001, * < 0.05; n.s., non-significant. In boxplots, the central marker (line) indicates the median

ion channels can also contribute to the differences in MN physiology. The low activation voltages of KV7_{2/3} channels^{53,57,6} play an increasingly important role in determining the inputoutput function of MN-R, the closer their membrane voltage is driven toward the AP threshold. Accordingly, we hypothesize that as the fraction of recruited KV7_{2/3} conductivity becomes larger, the closer depolarization drives MN-R toward their firing threshold. However, rheobase currents were not significantly lowered after blocking KV7_{2/3} channels, indicating that the higher leakiness of MN-R involves additional ion channels. A candidate to underly this leakiness is the ATP-sensitive potassium channel K_{ATP}. The significantly increased expression of ABCC9 transcript in MN-R might facilitate membrane-availability of K_{ATP} channels: proteins coded by ABCC9 and ABCC8 are regulatory subunits that form functional KATP channels in association with Kir6 proteins, ^{76–78} modulate K_{ATP} sensitivity to ATP, and are mandatory for membrane trafficking of the channel. 78-80

Single-cell sequencing also revealed a higher expression of RNA coding for the partially voltage-sensitive 81,82 sodium leak channel NALCN in MN-L. As NALCN determines neuron excitability and increases the excitability of neural networks, 83-85 an increased availability of voltage-dependent NALCN sodium flow that masks charges lost by KATP and depolarization-triggered M-type potassium outflow could diminish the influence of KV72/3 and KATP on shaping the MN-L sub-threshold inputoutput function. Interestingly and as expected by the existence of an additional sodium leak current, the mean RMP of MN-L was significantly higher than that of MN-R, indicating that NALCN abundance in the membrane of MN-L might indeed be higher than that in MN-R. Therefore, a combination of increased potassium outflow through functionally modified KV72/3 and $K_{\mbox{\scriptsize ATP}}$ channels and the loss of NALCN sodium inward currents in MN-R might be the fundament of the physiological differences between MN-R and MN-L.

Besides KV7_{2/3} and KV1₁, other channels likely contribute to the physiological differences between MN-L and MN-R. As our data demonstrate, differences exist not only in basal membrane properties and rheobase between MN-L and MN-R but also in their action potential properties and maximum firing frequency. High voltage-activated potassium channels such as KV3₁ are likely candidates to underlie such differences. Although our single-cell sequencing did not provide evidence for differential expression of any such high voltage-gated KV channels, their functionality might still be modulated by other mechanisms, such as alternative splicing or posttranslational modification.

Determination of MN transcriptional landscape in different parts of the rattlesnake spinal cord

Our single-cell sequencing revealed differential expression of RNA coding for NALCN channels and ABCC9 subunits, two candidates that might play into the different physiological features of MN activity. However, our patch-clamp results also demonstrate

value, and the bottom and top edges of the box show the 25th and 75th percentiles, respectively. For analysis, see STAR Methods. For bulk sequencing and qPCR of locomotor and rattle spinal cord, see Figures S5 and S6 and Tables S1–S4. For summary of all differentially expressed genes identified in single cell-sequencing, see Table S5.



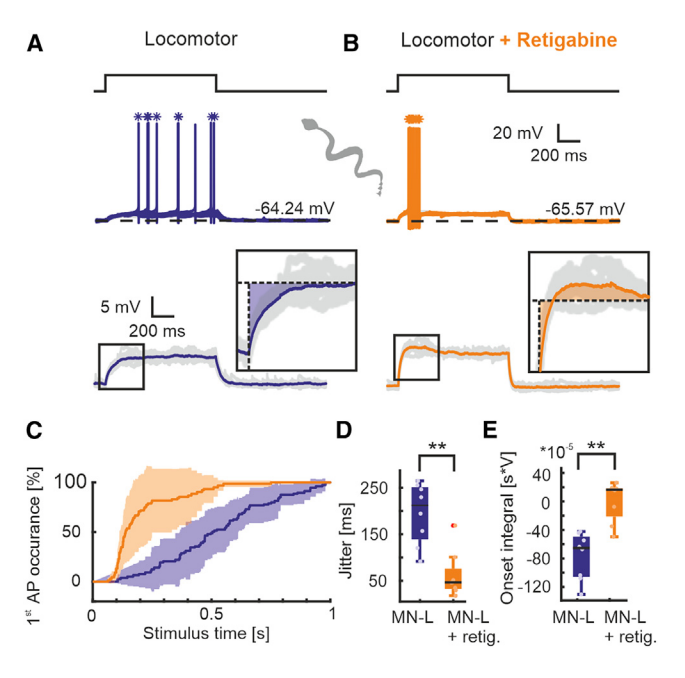


Figure 7. KV7_{2/3} channel enhancement superimposes rattle MN characteristics on locomotor MNs

(A and B) Traces recorded from a MN-L stimulated at rheobase current grouped into firing (top) and non-firing (bottom) repetitions. Note the differences in the course of onset voltages (bottom traces and insets) before (A) and after (B) application of retigabine. Under retigabine, first APs (* in A and B) shifted toward the stimulus onset.

(C-E) Under retigabine treatment, MN-L onset latency (C) and first AP jitter (D) were significantly reduced. Integrals between recording traces and equilibrium potentials after stimulus onset significantly increased (E). Statistics: Wilcoxon signed-rank test. p values: ** < 0.01. In boxplots, the central marker (line) indicates the median value, and the bottom and top edges of the box show the 25th and 75th percentiles, respectively. For additional data on XE991 modulation of MN membrane properties, see Figure S7.

that significant changes in MN physiology in the tail and body spinal cord of rattlesnakes heavily rely on KV72/3. However, these differences occur without major changes in the expression profile of KV7_{2/3} channels. Instead, we found several other effectors differentially expressed that can impact (KV7_{2/3}-) channel physiology, e.g., based on posttranslational phosphorylation. What could be the basis of this differential expression? One possible underlying regulator is the maintained elevated expression of HOXD9 in MN-R, when compared with MN-L. Hox genes and associated transcription factors have important roles in orchestrating the development of neural tissues and muscle innervation along animals' rostro-caudal body axis.86-90 However, evidence accumulated that Hox genes continue to be expressed in post-embryonic stages 91-93 and that they may play an important role to determine the transcriptional landscape of neurons that is needed for terminal differentiation after development. 94-98 The role of such transcription regulators in assigning sustained molecular identity of MNs in different parts of the spinal cord during adulthood remains to be fully understood. It appears likely that both mechanisms, the up- and down-regulation of expression of (ion-channel) proteins as well as their posttranslational modification, are important to adapt MN physiology for different behaviors.

Potential off-target effects of XE991 and retigabine

XE991 is a M-current blocker^{57,99–105} that has limited effects on other ion channels such as KV43, KV101 (eag1), and KV21. However, these side effects require higher drug concentrations and stronger depolarization than needed to activate the M-current.^{57,99} It is therefore unlikely that such off-target effects impacted our recordings. Retigabine enhances M-currents by increasing the opening probability of KV7_{2/3} channels.⁵³ Its off-target effects also unlikely affect our recordings, as concentrations effective in blocking other KV channels are several magnitudes higher (30-300 μM) than those required for KV7_{2/3} enhancement (1-10 μM). 106 Only KV21 channels are partially blocked by retigabine at concentrations in the range used in our study. However, their high voltage activation makes it unlikely that they modified the onset properties of the MN-Ls under retigabine treatment.

Can MN adaptation provide a driving force for the evolution of novel motor behaviors?

Changes in network connectivity, interneuron composition, and neuron physiology all contribute to CPG differences and thus to different behaviors. Our results suggest that the influence of potassium currents on MN activity can be varied through a combination of different mechanisms that do not necessarily involve major changes in expression profiles, as none of the voltage-gated potassium channel transcripts showed significant differences in expression. Nonetheless, KV7_{2/3} still heavily affected MN physiology. A shift in the transcriptional landscape that enhances KV7_{2/3} influence by posttranslational phosphorylation and also elevates the expression of NALCN and specific K_{ATP} subunits could thus be partially responsible for changing MN excitability and facilitate the integration of interneuron input as well as sustained ongoing AP firing in the respective behavioral time domains. The interplay of these changes applies a filter for the precision and timing of CPG motor output at the MN level (phasic vs. tonic firing). Such changes cannot only serve to evolve completely novel motor behaviors, as in the case of rattlesnakes, but presumably also help specialize the specific sub-divisions of spinal CPGs to control locomotion in different frequency ranges in general, as has been shown in zebrafish. 6,27,107 Although the evolution of CPGs that control the snakes' rattling muscles also requires adaptations at the interneuron network level, MNs, due to their function in transmitting CPG output to the muscles, need to feature suitable filter characteristics and physiological properties to allow the execution of adequate motor commands. Thus, even small physiological changes at the MN level might provide an important factor for the evolution of novel behaviors by altering CPG output sufficiently to impact the phenotype of locomotor behaviors.

STAR*METHODS

Detailed methods are provided in the online version of this paper and include the following:

- KEY RESOURCES TABLE
- **RESOURCE AVAILABILITY**
 - Lead contact
 - Materials availability

Article



- Data and code availability
- EXPERIMENTAL MODEL AND STUDY PARTICIPANT DE-**TAILS**
- METHOD DETAILS
 - o EMG recordings
 - Spinal cord preparation
 - O Spinal root backfills
 - In vitro slice physiology
 - O Stimulus protocols
 - Pharmacology
 - Single cell RNA sequencing
 - Bulk RNA sequencing
 - Whole cord qPCR
- QUANTIFICATION AND STATISTICAL ANALYSIS
 - In-vitro slice physiology
 - Single cell RNA sequencing
 - Bulk RNA sequencing
 - Whole cord qPCR

SUPPLEMENTAL INFORMATION

Supplemental information can be found online at https://doi.org/10.1016/j. cub.2023.11.062.

A video abstract is available at https://doi.org/10.1016/j.cub.2023.11. 062#mmc3.

ACKNOWLEDGMENTS

We thank members of the W. Enard laboratory for processing the single-cell RNA-seq and T. Royeck for drawings of locomotor and rattle pictograms. We acknowledge the usage of facilities and equipment from B. Grothe, D. Freitak, H. Luksch, and H. Straka. Funding of this study was provided from the DFG to B.P.C. (857/2-1).

AUTHOR CONTRIBUTIONS

B.P.C. conceptualized the study. M.S.B. and B.P.C. planned and performed patch-clamp experiments. M.S.B., B.P.C., and F.F. analyzed patch-clamp data. M.S.B. and B.P.C. conducted and analyzed in vitro backfills. B.P.C. and J.G. conducted single-cell and bulk-sequencing experiments. J.G. analyzed sequencing data. M.S.B. and J.G. conducted and analyzed qPCR experiments. M.S.B. and T.K. performed and analyzed in vivo EMG recordings of rattlesnakes. M.S.B. wrote the original draft of the manuscript. All authors critically proofread, discussed, and edited the manuscript.

DECLARATION OF INTERESTS

The authors declare no conflict of interests.

INCLUSION AND DIVERSITY

We support inclusive, diverse, and equitable conduct of research.

Received: July 19, 2023 Revised: October 11, 2023 Accepted: November 29, 2023 Published: December 28, 2023

REFERENCES

- 1. Grillner, S., Perret, C., and Zangger, P. (1976). Central generation of locomotion in the spinal dogfish. Brain Res. 109, 255-269.
- 2. Green, M.H., and Hale, M.E. (2012). Activity of pectoral fin motoneurons during two swimming gaits in the larval zebrafish (Danio rerio) and localization of upstream circuit elements. J. Neurophysiol. 108, 3393-3402.

- 3. Roberts, A., Soffe, S.R., Wolf, E.S., Yoshida, M., and Zhao, F.Y. (1998). Central circuits controlling locomotion in young frog tadpoles. Ann. N. Y. Acad. Sci. 860, 19-34.
- 4. Roberts, A., Li, W.C., and Soffe, S.R. (2010). How neurons generate behavior in a hatchling amphibian tadpole: an outline. Front. Behav. Neurosci. 4, 16.
- 5. Grillner, S., and El Manira, A. (2020). Current principles of motor control, with special reference to vertebrate locomotion. Physiol. Rev. 100,
- 6. Ampatzis, K., Song, J., Ausborn, J., and El Manira, A. (2013). Pattern of innervation and recruitment of different classes of motoneurons in adult zebrafish. J. Neurosci. 33, 10875-10886.
- 7. Grillner, S., and Wallén, P. (1984). How does the lamprey central nervous system make the lamprey swim? J. Exp. Biol. 112, 337-357.
- 8. Sholomenko, G.N., Funk, G.D., and Steeves, J.D. (1991). Locomotor activities in the decerebrate bird without phasic afferent input. Neuroscience 40, 257-266
- 9. Jacobson, R.D., and Hollyday, M. (1982). Electrically evoked walking and fictive locomotion in the chick. J. Neurophysiol. 48, 257-270.
- 10. Grillner, S., and Zangger, P. (1979). On the central generation of locomotion in the low spinal cat. Exp. Brain Res. 34, 241-261.
- 11. Kiehn, O., and Butt, S.J.B. (2003). Physiological, anatomical and genetic identification of CPG neurons in the developing mammalian spinal cord. Prog. Neurobiol. 70, 347-361.
- 12. Fish, F.E. (1998). Comparative kinematics and hydrodynamics of odontocete cetaceans: morphological and ecological correlates with swimming performance. J. Exp. Biol. 201, 2867-2877.
- 13. Sillar, K.T., and Roberts, A. (1993). Control of frequency during swimming in Xenopus embryos: a study on interneuronal recruitment in a spinal rhythm generator. J. Physiol. 472, 557-572.
- 14. Altshuler, D.L., and Dudley, R. (2003). Kinematics of hovering hummingbird flight along simulated and natural elevational gradients. J. Exp. Biol. 206, 3139-3147.
- 15. Chai, P., and Millard, D. (1997). Flight and size constraints: hovering performance of large hummingbirds under maximal loading. J. Exp. Biol.
- 16. Tobalske, B.W., Warrick, D.R., Clark, C.J., Powers, D.R., Hedrick, T.L., Hyder, G.A., and Biewener, A.A. (2007). Three-dimensional kinematics of hummingbird flight. J. Exp. Biol. 210, 2368-2382.
- 17. Pennycuick, C.J. (2001). Speeds and wingbeat frequencies of migrating birds compared with calculated benchmarks. J. Exp. Biol. 204, 3283-3294.
- 18. Hudson, P.E., Corr, S.A., and Wilson, A.M. (2012). High speed galloping in the cheetah (Acinonyx jubatus) and the racing greyhound (Canis familiaris): spatio-temporal and kinetic characteristics. J. Exp. Biol. 215, 2425-2434.
- 19. Nyakatura, J.A., Petrovitch, A., and Fischer, M.S. (2010). Limb kinematics during locomotion in the two-toed sloth (Choloepus didactylus, Xenarthra) and its implications for the evolution of the sloth locomotor apparatus. Zoology (Jena) 113, 221-234.
- 20. Kiehn, O. (2006). Locomotor circuits in the mammalian spinal cord. Annu. Rev. Neurosci. 29, 279-306.
- 21. Katz, P.S. (2016). Evolution of central pattern generators and rhythmic behaviours. Philos. Trans. R. Soc. Lond. B Biol. Sci. 371, 20150057.
- 22. Song, J., Pallucchi, I., Ausborn, J., Ampatzis, K., Bertuzzi, M., Fontanel, P., Picton, L.D., and El Manira, A. (2020). Multiple rhythm-generating circuits act in tandem with pacemaker properties to control the start and speed of locomotion. Neuron 105, 1048-1061.e4.
- 23. El Manira, A. (2014). Dynamics and plasticity of spinal locomotor circuits. Curr. Opin. Neurobiol. 29, 133-141.
- 24. Eklöf-Ljunggren, E., Haupt, S., Ausborn, J., Dehnisch, I., Uhleń, P., Higashijima, S.I., and El Manira, A. (2012). Origin of excitation underlying

Please cite this article in press as: Bothe et al., Timing and precision of rattlesnake spinal motoneurons are determined by the KV7_{2/3} potassium channel, Current Biology (2023), https://doi.org/10.1016/j.cub.2023.11.062



Current Biology Article

- locomotion in the spinal circuit of zebrafish. Proc. Natl. Acad. Sci. USA 109, 5511–5516.
- Ljunggren, E.E., Haupt, S., Ausborn, J., Ampatzis, K., and El Manira, A. (2014). Optogenetic activation of excitatory premotor interneurons is sufficient to generate coordinated locomotor activity in larval zebrafish. J. Neurosci. 34, 134–139.
- Fetcho, J.R., and McLean, D.L. (2010). Some principles of organization of spinal neurons underlying locomotion in zebrafish and their implications. Ann. N. Y. Acad. Sci. 1198, 94–104.
- McLean, D.L., Fan, J., Higashijima, S.I., Hale, M.E., and Fetcho, J.R. (2007). A topographic map of recruitment in spinal cord. Nature 446, 71–75.
- McLean, D.L., Masino, M.A., Koh, I.Y.Y., Lindquist, W.B., and Fetcho, J.R. (2008). Continuous shifts in the active set of spinal interneurons during changes in locomotor speed. Nat. Neurosci. 11, 1419–1429.
- Ritter, D.A., Bhatt, D.H., and Fetcho, J.R. (2001). In vivo imaging of zebrafish reveals differences in the spinal networks for escape and swimming movements. J. Neurosci. 21, 8956–8965.
- Bhatt, D.H., McLean, D.L., Hale, M.E., and Fetcho, J.R. (2007). Grading movement strength by changes in firing intensity versus recruitment of spinal interneurons. Neuron 53, 91–102.
- Henneman, E. (1957). Relation between size of neurons and their susceptibility to discharge. Science 126, 1345–1347.
- Henneman, E., Somjen, G., and Carpenter, D.O. (1965). Functional significance of cell size in spinal motoneurons. J. Neurophysiol. 28, 560–580.
- **33.** Moon, B.R., and Gans, C. (1998). Kinematics, muscular activity and propulsion in gopher snakes. J. Exp. Biol. *201*, 2669–2684.
- 34. Jayne, B.C. (2020). What defines different modes of snake locomotion? Integr. Comp. Biol. 60, 156–170.
- Moon, B.R. (2000). The mechanics and muscular control of constriction in gopher snakes (*Pituophis melanoleucus*) and a king snake (*Lampropeltis getula*). J. Zool. 252, 83–98.
- Jayne, B.C. (1988). Muscular mechanisms of snake locomotion: an electromyographic study of lateral undulation of the florida banded water snake (*Nerodia fasciata*) and the yellow rat snake (*Elaphe obsoleta*).
 J. Morphol. 197, 159–181.
- Chadwick, L.E., and Rahn, H. (1954). Temperature dependence of rattling frequency in the rattlesnake *Crotalus v. viridis*. Science 119, 442–443.
- Forsthofer, M., Schutte, M., Luksch, H., Kohl, T., Wiegrebe, L., and Chagnaud, B.P. (2021). Frequency modulation of rattlesnake acoustic display affects acoustic distance perception in humans. Curr. Biol. 31, 4367–4372.e4.
- Smith, J.L., Edgerton, V.R., Betts, B., and Collatos, T.C. (1977). EMG of slow and fast ankle extensors of cat during posture, locomotion, and jumping. J. Neurophysiol. 40, 503–513.
- Guimaraes, A.C., Herzog, W., Allinger, T.L., and Zhang, Y.T. (1995). The EMG-force relationship of the cat soleus muscle and its association with contractile conditions during locomotion. J. Exp. Biol. 198, 975–987.
- Dial, K.P., Kaplan, S.R., Goslow, G.E., and Jenkins, F.A. (1988). A functional analysis of the primary upstroke and downstroke muscles in the domestic pigeon (*Columba livia*) during flight. J. Exp. Biol. 134, 1–16.
- Lutz, G.J., and Rome, L.C. (1996). Muscle function during jumping in frogs. I. Sarcomere length change, EMG pattern, and jumping performance. Am. J. Physiol. 271, C563–C570.
- Scholle, H.C., Biedermann, F., Arnold, D., Jinnah, H.A., Grassme, R., and Schumann, N.P. (2005). A surface EMG multi-electrode technique for characterizing muscle activation patterns in mice during treadmill locomotion. J. Neurosci. Methods 146, 174–182.
- Martin, J.H., and Bagby, R.M. (1973). Properties of rattlesnake shaker muscle. J. Exp. Zool. 185, 293–300.

- Schaeffer, P.J., Conley, K.E., and Lindstedt, S.T. (1996). Structural correlates of speed and endurance in skeletal muscle: the rattlesnake tail-shaker muscle. J. Exp. Biol. 199, 351–358.
- 46. Glazebrook, P.A., Ramirez, A.N., Schild, J.H., Shieh, C.C., Doan, T., Wible, B.A., and Kunze, D.L. (2002). Potassium channels Kv1.1, Kv1.2 and Kv1.6 influence excitability of rat visceral sensory neurons. J. Physiol. 541, 467–482.
- Chi, X.X., and Nicol, G.D. (2007). Manipulation of the potassium channel Kv1.1 and its effect on neuronal excitability in rat sensory neurons. J. Neurophysiol. 98, 2683–2692.
- Gittelman, J.X., and Tempel, B.L. (2006). Kv1.1-containing channels are critical for temporal precision during spike initiation. J. Neurophysiol. 96, 1203–1214.
- Kopp-Scheinpflug, C., Fuchs, K., Lippe, W.R., Tempel, B.L., and Rübsamen, R. (2003). Decreased temporal precision of auditory signaling in Kcna1-null mice: an electrophysiological study in vivo. J. Neurosci. 23, 9199–9207.
- Lombardo, J., and Harrington, M.A. (2016). Nonreciprocal mechanisms in up- and downregulation of spinal motoneuron excitability by modulators of KCNQ/Kv7 channels. J. Neurophysiol. 116, 2114–2124.
- Verneuil, J., Brocard, C., Trouplin, V., Villard, L., Peyronnet-Roux, J., and Brocard, F. (2020). The M-current works in tandem with the persistent sodium current to set the speed of locomotion. PLOS Biol. 18, e3000738.
- Alaburda, A., Perrier, J.F., and Hounsgaard, J. (2002). An M-like outward current regulates the excitability of spinal motoneurones in the adult turtle. J. Physiol. 540, 875–881.
- Wickenden, A.D., Yu, W., Zou, A., Jegla, T., and Wagoner, P.K. (2000).
 Retigabine, a novel anti-convulsant, enhances activation of KCNQ2/Q3 potassium channels. Mol. Pharmacol. 58, 591–600.
- Rome, L.C. (2006). Design and function of superfast muscles: new insights into the physiology of skeletal muscle. Annu. Rev. Physiol. 68, 193–221.
- Rome, L.C., and Lindstedt, S.L. (1998). The quest for speed: muscles built for high-frequency contractions. News Physiol. Sci. 13, 261–268.
- Brown, D.A., and Adams, P.R. (1980). Muscarinic suppression of a novel voltage-sensitive K+ current in a vertebrate neurone. Nature 283, 673–676.
- Wang, H.S., Pan, Z., Shi, W., Brown, B.S., Wymore, R.S., Cohen, I.S., Dixon, J.E., and McKinnon, D. (1998). KCNQ2 and KCNQ3 potassium channel subunits: molecular correlates of the M-channel. Science 282, 1890–1893
- Carver, C.M., and Shapiro, M.S. (2019). Gq-coupled muscarinic receptor enhancement of KCNQ2/3 channels and activation of TRPC channels in multimodal control of excitability in dentate gyrus granule cells. J. Neurosci. 39, 1566–1587.
- Zhang, J., and Shapiro, M.S. (2012). Activity-dependent transcriptional regulation of M-type (Kv7) K+ channels by AKAP79/150-mediated NFAT actions. Neuron 76, 1133–1146.
- Wu, W.W., Chan, C.S., Surmeier, D.J., and Disterhoft, J.F. (2008). Coupling
 of L-type Ca2+ channels to KV7/KCNQ channels creates a novel, activitydependent, homeostatic intrinsic plasticity. J. Neurophysiol. 100,
 1897–1908.
- Stewart, A.P., Gómez-Posada, J.C., McGeorge, J., Rouhani, M.J., Villarroel, A., Murrell-Lagnado, R.D., and Edwardson, J.M. (2012). The Kv7.2/Kv7.3 heterotetramer assembles with a random subunit arrangement. J. Biol. Chem. 287, 11870–11877.
- 62. Schwake, M., Pusch, M., Kharkovets, T., and Jentsch, T.J. (2000). Surface expression and single channel properties of KCNQ2/KCNQ3, M-type K+ channels involved in epilepsy. J. Biol. Chem. 275, 13343– 13348.
- Selyanko, A.A., Hadley, J.K., and Brown, D.A. (2001). Properties of single M-type KCNQ2/KCNQ3 potassium channels expressed in mammalian cells. J. Physiol. 534, 15–24.

Article



- Etxeberria, A., Santana-Castro, I., Regalado, M.P., Aivar, P., and Villarroel, A. (2004). Three mechanisms underlie KCNQ2/3 heteromeric potassium M-channel potentiation. J. Neurosci. 24, 9146–9152.
- Gómez-Posada, J.C., Etxeberría, A., Roura-Ferrer, M., Areso, P., Masin, M., Murrell-Lagnado, R.D., and Villarroel, A. (2010). A pore residue of the KCNQ3 potassium M-channel subunit controls surface expression. J. Neurosci. 30. 9316–9323.
- Zaika, O., Hernandez, C.C., Bal, M., Tolstykh, G.P., and Shapiro, M.S. (2008). Determinants within the turret and pore-loop domains of KCNQ3 K+ channels governing functional activity. Biophys. J. 95, 5121–5137.
- Schroeder, B.C., Kubisch, C., Stein, V., and Jentsch, T.J. (1998).
 Moderate loss of function of cyclic-AMP-modulated KCNQ2/KCNQ3
 K+ channels causes epilepsy. Nature 396, 687–690.
- 68. Arnsten, A.F.T., Jin, L.E., Gamo, N.J., Ramos, B., Paspalas, C.D., Morozov, Y.M., Kata, A., Bamford, N.S., Yeckel, M.F., Kaczmarek, L.K., et al. (2019). Role of KCNQ potassium channels in stress-induced deficit of working memory. Neurobiol. Stress 11, 100187.
- van der Horst, J., Greenwood, I.A., and Jepps, T.A. (2020). Cyclic AMPdependent regulation of Kv7 voltage-gated potassium channels. Front. Physiol. 11, 727.
- Kosenko, A., Kang, S., Smith, I.M., Greene, D.L., Langeberg, L.K., Scott, J.D., and Hoshi, N. (2012). Coordinated signal integration at the M-type potassium channel upon muscarinic stimulation. EMBO J. 31, 3147–3156
- Salzer, I., Erdem, F.A., Chen, W.Q., Heo, S., Koenig, X., Schicker, K.W., Kubista, H., Lubec, G., Boehm, S., and Yang, J.W. (2017). Phosphorylation regulates the sensitivity of voltage-gated Kv7.2 channels towards phosphatidylinositol-4,5-bisphosphate. J. Physiol. 595, 759–776.
- Li, Y., Langlais, P., Gamper, N., Liu, F., and Shapiro, M.S. (2004). Dual phosphorylations underlie modulation of unitary KCNQ K(+) channels by Src tyrosine kinase. J. Biol. Chem. 279, 45399–45407.
- 73. Hoshi, N., Zhang, J.S., Omaki, M., Takeuchi, T., Yokoyama, S., Wanaverbecq, N., Langeberg, L.K., Yoneda, Y., Scott, J.D., Brown, D.A., et al. (2003). AKAP150 signaling complex promotes suppression of the M-current by muscarinic agonists. Nat. Neurosci. 6, 564–571.
- Michaeli, T., Bloom, T.J., Martins, T., Loughney, K., Ferguson, K., Riggs, M., Rodgers, L., Beavo, J.A., and Wigler, M. (1993). Isolation and characterization of a previously undetected human cAMP phosphodiesterase by complementation of cAMP phosphodiesterase-deficient Saccharomyces cerevisiae. J. Biol. Chem. 268, 12925–12932.
- Kim, K.S., Duignan, K.M., Hawryluk, J.M., Soh, H., and Tzingounis, A.V. (2016). The voltage activation of cortical KCNQ channels depends on global PIP2 Levels. Biophys. J. 110, 1089–1098.
- Hibino, H., Inanobe, A., Furutani, K., Murakami, S., Findlay, I., and Kurachi, Y. (2010). Inwardly rectifying potassium channels: their structure, function, and physiological roles. Physiol. Rev. 90, 291–366.
- Nelson, P.T., Jicha, G.A., Wang, W.X., Ighodaro, E., Artiushin, S., Nichols, C.G., and Fardo, D.W. (2015). ABCC9/SUR2 in the brain: implications for hippocampal sclerosis of aging and a potential therapeutic target. Ageing Res. Rev. 24, 111–125.
- Nichols, C.G. (2006). KATP channels as molecular sensors of cellular metabolism. Nature 440, 470–476.
- Neagoe, I., and Schwappach, B. (2005). Pas de deux in groups of fourthe biogenesis of KATP channels. J. Mol. Cell. Cardiol. 38, 887–894.
- Bryan, J., Muñoz, A., Zhang, X., Düfer, M., Drews, G., Krippeit-Drews, P., and Aguilar-Bryan, L. (2007). ABCC8 and ABCC9: ABC transporters that regulate K+ channels. Pflugers Arch. 453, 703–718.
- Chua, H.C., Wulf, M., Weidling, C., Rasmussen, L.P., and Pless, S.A. (2020). The NALCN channel complex is voltage sensitive and directly modulated by extracellular calcium. Sci. Adv. 6, eaaz3154.
- 82. Kang, Y., and Chen, L. (2022). Structure and mechanism of NALCN-FAM155A-UNC79-UNC80 channel complex. Nat. Commun. 13, 2639.

- 83. Lu, B., Su, Y., Das, S., Liu, J., Xia, J., and Ren, D. (2007). The neuronal channel NALCN contributes resting sodium permeability and is required for normal respiratory rhythm. Cell 129, 371–383.
- 84. Philippart, F., and Khaliq, Z.M. (2018). G i/o protein-coupled receptors in dopamine neurons inhibit the sodium leak channel NALCN. eLife 7, 1–19.
- Gao, S., Xie, L., Kawano, T., Po, M.D., Guan, S., Zhen, M., Pirri, J.K., and Alkema, M.J. (2015). The NCA sodium leak channel is required for persistent motor circuit activity that sustains locomotion. Nat. Commun. 6, 6323.
- Miller, A., and Dasen, J.S. (2024). Establishing and maintaining Hox profiles during spinal cord development. Semin. Cell Dev. Biol. 152– 153, 44–57.
- Jung, H., Mazzoni, E.O., Soshnikova, N., Hanley, O., Venkatesh, B., Duboule, D., and Dasen, J.S. (2014). Evolving hox activity profiles govern diversity in locomotor systems. Dev. Cell 29, 171–187.
- Dasen, J.S., De Camilli, A., Wang, B., Tucker, P.W., and Jessell, T.M. (2008). Hox repertoires for motor neuron diversity and connectivity gated by a single accessory factor, FoxP1. Cell 134, 304–316.
- 89. Philippidou, P., and Dasen, J.S. (2013). Hox Genes: choreographers in neural development, architects of circuit organization. Neuron 80, 12–34.
- Jung, H., Baek, M., D'Elia, K.P., Boisvert, C., Currie, P.D., Tay, B.H., Venkatesh, B., Brown, S.M., Heguy, A., Schoppik, D., et al. (2018). The ancient origins of neural substrates for land walking. Cell 172, 667– 682.e15.
- Joshi, R., Sipani, R., and Bakshi, A. (2022). Roles of drosophila Hox genes in the assembly of neuromuscular networks and behavior. Front. Cell Dev. Biol. 9. 786993.
- Feng, W., Destain, H., Smith, J.J., and Kratsios, P. (2022). Maintenance of neurotransmitter identity by Hox proteins through a homeostatic mechanism. Nat. Commun. 13, 6097.
- 93. Rux, D.R., and Wellik, D.M. (2017). Hox genes in the adult skeleton: novel functions beyond embryonic development. Dev. Dyn. 246, 310–317.
- 94. Catela, C., Chen, Y., Weng, Y., Wen, K., and Kratsios, P. (2022). Control of spinal motor neuron terminal differentiation through sustained Hoxc8 gene activity. eLife 11.
- Hutlet, B., Theys, N., Coste, C., Ahn, M.T., Doshishti-Agolli, K., Lizen, B., and Gofflot, F. (2016). Systematic expression analysis of Hox genes at adulthood reveals novel patterns in the central nervous system. Brain Struct. Funct. 221, 1223–1243.
- Awgulewitsch, A., and Jacobs, D. (1990). Differential expression of Hox 3.1 protein in subregions of the embryonic and adult spinal cord. Development 108, 411–420.
- Coughlan, E., Garside, V.C., Wong, S.F.L., Liang, H., Kraus, D., Karmakar, K., Maheshwari, U., Rijli, F.M., Bourne, J., and McGlinn, E. (2019). A Hox code defines spinocerebellar neuron subtype regionalization. Cell Rep. 29, 2408–2421.e4.
- 98. Hobert, O. (2011). Regulation of terminal differentiation programs in the nervous system. Annu. Rev. Cell Dev. Biol. 27, 681–696.
- Wladyka, C.L., and Kunze, D.L. (2006). KCNQ/M-currents contribute to the resting membrane potential in rat visceral sensory neurons. J. Physiol. 575, 175–189.
- 100. Bordas, C., Kovacs, A., and Pal, B. (2015). The M-current contributes to high threshold membrane potential oscillations in a cell type-specific way in the pedunculopontine nucleus of mice. Front. Cell. Neurosci. 9, 121.
- 101. Gu, N., Vervaeke, K., Hu, H., and Storm, J.F. (2005). Kv7/KCNQ/M and HCN/h, but not KCa2/SK channels, contribute to the somatic medium after-hyperpolarization and excitability control in CA1 hippocampal pyramidal cells. J. Physiol. 566, 689–715.
- 102. Martire, M., Castaldo, P., D'Amico, M., Preziosi, P., Annunziato, L., and Taglialatela, M. (2004). M channels containing KCNQ2 subunits modulate norepinephrine, aspartate, and GABA release from hippocampal nerve terminals. J. Neurosci. 24, 592–597.
- Brown, D.A., and Passmore, G.M. (2009). Neural KCNQ (Kv7) channels.
 Br. J. Pharmacol. 156, 1185–1195.

Please cite this article in press as: Bothe et al., Timing and precision of rattlesnake spinal motoneurons are determined by the KV7_{2/3} potassium channel, Current Biology (2023), https://doi.org/10.1016/j.cub.2023.11.062



Current Biology

- 104. Miceli, F., Soldovieri, M.V., Martire, M., and Taglialatela, M. (2008). Molecular pharmacology and therapeutic potential of neuronal Kv7modulating drugs. Curr. Opin. Pharmacol. 8, 65-74.
- 105. Zhang, Y., Li, D., Darwish, Y., Fu, X., Trussell, L.O., and Huang, H. (2022). KCNQ channels enable reliable presynaptic spiking and synaptic transmission at high frequency. J. Neurosci. 42, 3305-3315.
- 106. Stas, J.I., Bocksteins, E., Jensen, C.S., Schmitt, N., and Snyders, D.J. (2016). The anticonvulsant retigabine suppresses neuronal KV2-mediated currents. Sci. Rep. 6, 35080.
- 107. Moreno, R.L., and Ribera, A.B. (2009). Zebrafish motor neuron subtypes differ electrically prior to axonal outgrowth. J. Neurophysiol. 102,
- 108. Bagnoli, J.W., Ziegenhain, C., Janjic, A., Wange, L.E., Vieth, B., Parekh, S., Geuder, J., Hellmann, I., and Enard, W. (2018). Sensitive and powerful single-cell RNA sequencing using mcSCRB-seq. Nat. Commun. 9, 2937.
- 109. Schindelin, J., Arganda-Carreras, I., Frise, E., Kaynig, V., Longair, M., Pietzsch, T., Preibisch, S., Rueden, C., Saalfeld, S., Schmid, B., et al. (2012). Fiji: an open-source platform for biological-image analysis. Nat. Methods 9, 676-682.
- 110. Lidierth, M. (2009). sigTOOL: a MATLAB-based environment for sharing laboratory-developed software to analyze biological signals. J. Neurosci. Methods 178, 188-196.
- 111. Westhoff, G. (2014). Giftschlangen und Krustenechsen. Sachkunde Gefährliche Reptilien, 9-55. VDA, and Sachkunde, D.G.H.T. GbR.
- 112. Savitzky, A.H., and Moon, B.R. (2008). Tail morphology in the western diamond-backed rattlesnake, Crotalus atrox. J. Morphol. 269, 935-944.

- 113. Parekh, S., Ziegenhain, C., Vieth, B., Enard, W., and Hellmann, I. (2018). zUMIs - A fast and flexible pipeline to process RNA sequencing data with UMIs. GigaScience 7.
- 114. Dobin, A., Davis, C.A., Schlesinger, F., Drenkow, J., Zaleski, C., Jha, S., Batut, P., Chaisson, M., and Gingeras, T.R. (2013). STAR: ultrafast universal RNA-seq aligner. Bioinformatics 29, 15-21.
- 115. Margres, M.J., Rautsaw, R.M., Strickland, J.L., Mason, A.J., Schramer, T.D., Hofmann, E.P., Stiers, E., Ellsworth, S.A., Nystrom, G.S., Hogan, M.P., et al. (2021). The tiger rattlesnake genome reveals a complex genotype underlying a simple venom phenotype. Proc. Natl. Acad. Sci. USA 118. e2014634118.
- 116. Hao, Y., Hao, S., Andersen-Nissen, E., Mauck, W.M., Zheng, S., Butler, A., Lee, M.J., Wilk, A.J., Darby, C., Zager, M., et al. (2021). Integrated analysis of multimodal single-cell data. Cell 184, 3573-3587.e29.
- 117. Bolger, A.M., Lohse, M., and Usadel, B. (2014). Trimmomatic: a flexible trimmer for Illumina sequence data. Bioinformatics 30, 2114-2120.
- 118. Li, B., and Dewey, C.N. (2011). RSEM: accurate transcript quantification from RNA-Seq data with or without a reference genome. BMC Bioinform.
- 119. Soneson, C., Love, M.I., and Robinson, M.D. (2015). Differential analyses for RNA-seq: transcript-level estimates improve gene-level inferences. F1000Res 4, 1521. version 2; peer review: 2 approved.
- 120. Love, M.I., Huber, W., and Anders, S. (2014). Moderated estimation of fold change and dispersion for RNA-seq data with DESeq2. Genome Biol. 15, 550.
- 121. Benjamini, Y., and Hochberg, Y. (1995). Controlling the false discovery rate: a practical and powerful approach to multiple testing. J. R. Stat. Soc. B 57, 289-300.

Please cite this article in press as: Bothe et al., Timing and precision of rattlesnake spinal motoneurons are determined by the KV7_{2/3} potassium channel, Current Biology (2023), https://doi.org/10.1016/j.cub.2023.11.062

Current Biology Article



STAR*METHODS

KEY RESOURCES TABLE

| REAGENT or RESOURCE | SOURCE | IDENTIFIER |
|--|-------------------------------|---|
| Chemicals, peptides, and recombinant proteins | | |
| XE991 dihydrochloride | Alomone Labs | Cat#X-101 |
| Retigabine dihydrochloride | Alomone Labs | Cat#R-101 |
| α-Dendrotoxin | Alomone Labs | Cat#D-350 |
| Critical commercial assays | | |
| Qiagen RNeasy Mini Kit | Qiagen | Cat#74104 |
| ROTIPrep RNA Mini Kit | Carlroth GmbH + Co. KG | Cat#8485.2 |
| Script cDNA Synthesis Kit | Bio-Rad Laboratories Inc. | Cat#1708890 |
| Q Multiplex Powermix | Bio-Rad Laboratories Inc. | Cat#1725848 |
| KAPA Illumina Library quantification kit | Roche Holding AG | Cat#07960140001 |
| TruSeq stranded mRNA Library preparation kit | Illumina | Cat#20020594 |
| Deposited data | | |
| RNA sequencing data | This paper | NCBI Bioproject: https://www.ncbi.nlm.nih.gov/bioproject/?term=PRJNA996101 |
| Electrophysiology data | This paper | Zenodo: https://doi.org/10.5281/zenodo. 10137298 |
| EMG data | This Paper | Zenodo: https://doi.org/10.5281/zenodo. 10137298 |
| Experimental models: Organisms/strains | | |
| Western Diamondback Rattlesnake (Crotalus atrox) | In-house breeding facility | N/A |
| Oligonucleotides | | |
| Oligo-dt primers for single cell sequencing | Bagnoli et al. ¹⁰⁸ | https://doi.org/10.1038/s41467-018-05347-6 |
| Primers for qPCR: See Table S4 | This paper | N/A |
| Software and algorithms | | |
| MATLAB, Ver. R2017b | The MathWorks, Inc. | RRID:SCR_001622 |
| Image J, FIJI distribution | Schindelin et al. 109 | RRID:SCR_002285 https://doi.org/10.1038/nmeth.2019 |
| CorelDRAW Graphics Suite 2021 | Cascade Parent Limited | RRID:SCR_014235 |
| NIS-Elements Br | Nikon Corporation | RRID:SCR_014329 |
| sigTOOL | Lidierth et al. 110 | https://sigtool.sourceforge.net/sigtool.html; https://doi.org/10.1016/j.jneumeth.2008.11.004 |
| Matlab-Patchmaster toolbox | Stanford Wormsenselab | https://github.com/wormsenseLab/ Matlab-PatchMaster |
| Other | | |
| Code | This paper | (https://doi.org/10.5281/zenodo.10137298) |

RESOURCE AVAILABILITY

Lead contact

Further information and requests for resources and reagents should be directed to and will be fulfilled by the lead contact, Maximilian Bothe (maximilian.bothe@uni-graz.at).

Materials availability

This study did not generate new unique reagents.

Please cite this article in press as: Bothe et al., Timing and precision of rattlesnake spinal motoneurons are determined by the KV72/3 potassium channel, Current Biology (2023), https://doi.org/10.1016/j.cub.2023.11.062





Data and code availability

RNAseq reads are deposited in the NCBI SRA database. The accession number is listed in the key resources table. Information on primers used for qPCR are provided in Table S4 in the supplemental information. Raw data of patch clamp recordings and parameters of applied stimuli are deposited at the Zenodo open repository. Raw EMG data are deposited at the Zenodo open repository. The DOI for accession is listed in the key resources table.

All code that was used for the analysis of sequencing and electrophysiological data is deposited at the Zenodo open repository. The DOI for accession is listed in the key resources table.

Any additional information required to reanalyze the data reported in this paper is available from the lead contact upon request.

EXPERIMENTAL MODEL AND STUDY PARTICIPANT DETAILS

Experiments were performed on 47 juvenile (age: 1- and 2-years old) western diamondback rattlesnakes, Crotalus atrox, of either sex that were group-housed (two to three snakes per terrarium) and kept on a 12:12-hour day:night cycle at a temperature of 25-31°C with water ad libitum. Animals were fed weekly with dead mice. All experimental animals were bred and kept at the Chair of Zoology of the Technical University of Munich, following the established guidelines for care and maintenance of venomous snakes. 111 Permission for animal experiments was granted by the respective governmental institution at the Regierung von Oberbayern (Gz: ROB-55.1-2532.Vet_02-19-115).

METHOD DETAILS

EMG recordings

Seven rattlesnakes (Crotalus atrox) of bodyweights between 82 and 445 g and snout to vent lengths between 44 and 112 cm were initially anaesthetized in an air-tight chamber by application of 0.1 ml isoflurane. To ensure a deep anesthesia throughout the entire implantation process, snakes were intubated with a cat catheter (diameter: 1.2 mm) and isoflurane was provided at a concentration of 2.0 – 2.5 % by an isoflurane vaporizer (Isotec-3, Völker GmbH Kaltenkirchen, Germany). For additional analgesic treatment, Carprofen (Caprosol, cp-pharma, Burgdorf, Germany) was administered (2 mg/kg body weight, i.m.) 1 h before the implantation process and the following day of EMG recording. After cessation of the tail pinch reflex, bilateral implantation of a total of 4 bipolar EMG-electrodes was performed. Electrodes were made from Omnetics 9 pin, pre-wired polarized COT connectors (NSD-09-WD-18.0-C-GS, Omnetics Connector Corporation, Minneapolis, USA), with a wire- length of 45 cm. 1-2 mm of insulation was removed from wires used for implantation and blank ends were implanted on locomotor and rattle muscles, respectively. Electrodes were positioned dorso-laterally, to lie subcutaneously within a visible groove between the musculus longissimus dorsi and the musculus iliocostalis. 112 To prevent entangling in or pulling out the cables when the animal woke up and during the actual EMG recordings, implanted wires were additionally fixed by surgical suture (Daclon Nylon, Monofilament Non-absorbable, USP 2/0, SMI AG, St. Vith, Belgium). After implantation, animals were kept in individual terraria and allowed to recover completely from surgery before EMG recordings started. For recordings, animals were fixed by their head by means of a snake hook and electrode cables were connected to an intan technologies RHD USB Interface board (RHD USB Interface board, intan Technologies, Los Angeles, USA), using a RHD 16-channel Recording headstage for preamplification (RHD 16-Channel Bipolar-Input Recording Headstage, intan Technologies, Los Angeles, USA). To allow for more moving space, electrode cables were daisy-chained with another set of cables (NPS-09-WD-18.0-C-GS, Omnetics Connector Corporation, Minneapolis, USA). For EMG recordings, animals were put into an arena (100 cm X 100 cm) and were either allowed to move freely or between two barriers, to enforce rectilinear locomotion. Rattling was triggered by presenting the animals with a circular (Ø = 8.9 mm) 1.3 W IR emitter (Steady State IR Source, Model EK-5270, Laser Components GmbH, Olching, Germany, max. radiation density at 2.5 mm), mounted to a wooden bar of 1.5 m length. Data was recorded using the freely available USB interface board software (USB Interface Board software v 1.5.4, intan Technologies, Los Angeles, USA), subsequently imported (MATLAB RHD file reader, intan Technologies, Los Angeles, USA) to MATLAB (Matlab2017b, The MathWorks, Massachusetts, USA) and analyzed using custom written scripts. Twenty low-noise representations of individual locomotor events were extracted from EMG recordings of locomotor muscles. For the analysis of shaker EMG activity, three times two seconds of EMG activity were extracted from each respective experimental animal.

Spinal cord preparation

25 Rattlesnakes (Crotalus atrox) of bodyweights between 20 and 56 g and snout to vent lengths between 33.5 and 49.5 cm were anaesthetized (see above) and after cessation of the tail pinch reflex decapitated and subsequently perfused transcardially with ice-cold, oxygenated snake Ringer solution (in mM | 11: 96.5 NaCl, 31.5 NaHCO3, 2 CaCl2, 2.6 KCL, 2 MgCl2 and 20 D-glucose, pH 7.4). As soon as the blood was completely replaced by ringer solution, ~2 cm long segments of thoracic and tail spinal cord were dissected for probing locomotor and rattle spinal networks, respectively. To access the spinal cord, muscle tissue was removed from the spinal column before the bone was opened from the dorsal side to allow ringer diffusion. In this state, the tissue was stored free-floating for up to 4 days in oxygenated snake ringer solution at 4°C. Before recordings, bone surrounding the spinal segments was completely removed to use either whole spinal cord preparations for ventral root backfills or enable tissue slicing.

Please cite this article in press as: Bothe et al., Timing and precision of rattlesnake spinal motoneurons are determined by the KV7_{2/3} potassium channel, Current Biology (2023), https://doi.org/10.1016/j.cub.2023.11.062

Current Biology Article



Spinal root backfills

To visualize motoneurons (MNs) in locomotor and rattle spinal cord, we applied fluorophore coupled dextran (Dextran, Alexa Fluor 488, 546; 3000 MW, Thermo Fisher Scientific, Invitrogen) to spinal root nerves of whole spinal cord preparations from seven animals. Spinal cord segments were taken from animals that were also used for patch clamp electrophysiology. Three to four segments of spinal cord were dissected out of the vertebral column and care was taken to preserve as much of the ventral roots as possible. The nerves were surrounded by petroleum jelly (Vaseline weiß, Bombastus-Werke, 01705 Freital, Germany) and Ringer solution was removed from the inside of the formed well. Crystals of the dextran dyes were then applied to the blunt nerve ends. After 15 minutes of incubation time, excess dye was sucked off with a tissue wipe and the nerves were washed with Ringer solution. Preparations were then incubated in Ringer solution for 24-48 hours at 7°C. After incubation, tissue was fixed in 4% paraformaldehyde overnight and subsequently cut to 60 or 100 μm slices with a vibratome (Ci 7000 SMZ 2, Campden Instruments, Loughborough, England). Slices were imaged using a fluorescence stereomicroscope (Nikon SMZ 25, Nikon Europe B.V. 1120 Wien, Austria) equipped with a monochrome camera (DMK33UX174, The Imaging Source GmbH, 28217 Bremen, Germany) and the NIS Elements Br software (NIS Elements Br, Nikon Europe B.V. 1120 Wien, Austria). Analysis was done using ImageJ (FIJI distribution¹⁰⁹).

In vitro slice physiology Slice preparation

To allow for a visual approach of individual motoneurons, 200 μm spinal cord slices were cut from whole spinal cord preparations (see above). Spinal cord segments were embedded in 2 % low melting point agar (Agarose Low-Melt, Carl Roth GmbH + Co. KG, 76185 Karlsruhe, Germany) and rapidly cooled down. The agar-embedded tissue was cut in ice-cold slice solution (in mM: Sucrose: 50, NaCl: 25, NaHCO₃: 27, KCl: 2.5, MgCl₂: 3, CaCl₂: 0.1, glucose: 25, ascorbic acid: 0.4, Myoinositol: 3, Na-pyruvate: 2) using a vibratome (Ci 7000 SMZ 2, Campden Instruments, Loughborough, England). After cutting, each slice was directly transferred to an incubation chamber filled with oxygenated recording solution (in mM: same as slice solution but adding 125 mM NaCl, 2 mM CaCl₂, 1mM MgCl₂ and no sucrose). To allow for tissue recovery, slices were kept at room temperature for 30 minutes before recordings started.

Recording setup and electrodes

For patch clamp electrophysiology, slices were transferred to a recording chamber and continuously superfused with patch clamp recording solution (see above) at room temperature. Motoneurons were visualized through a microscope (Zeiss Examiner.A1, Carl Zeiss Microscopy Deutschland, 73446 Oberkochen, Germany) with Dodt contrast and a 1.0 NA objective (Zeiss 40x/1.0 DIC VIS-IR, Carl Zeiss Microscopy Deutschland, 73446 Oberkochen, Germany). Slices were visualized for patching with a digital CMOS camera (Orca flash 4.0 LT, C11440, Hamamatsu Photonics K.K., Hamamatsu, Japan). Recorded signals were amplified and digitized with a patch clamp amplifier (HEKA EPC 10 USB, HEKA Elektronik GmbH, 72770 Reutlingen, Germany) at 100 kHz sampling rate and visualized in the Patchmaster Software (HEKA Patchmaster, HEKA Elektronik GmbH, 72770 Reutlingen, Germany). Analysis of the recordings was performed in Matlab (MATLAB, R2017b, The MathWorks, Natick Massachusetts, USA). All neurons that did not require a holding current (before applying blockers/enhancers) and that stayed stable over the course of an experiment, were used for analysis. To load Patchmaster files into Matlab the "sigTool¹¹⁰" and "Matlab-patchmaster" toolboxes (see key resources table) were used.

Patch electrodes were pulled with a micropipette puller (DMZ-Universal-Electrode-Puller, Zeitz Instrumente Vertriebs GmbH, Bavaria, Germany or P-87 Micropipette Puller, Sutter Instrument, California, USA) and filled with patch solution (in mM: K-gluconate 145, KCl 4.5, HEPES 15, Mg-ATP 2, K_2 -ATP dihydrate 2, Na_2 -GTP 0.3, Na_2 -Phosphocreatine 7.5) to reach a final resistance of 4-9 $M\Omega$. The liquid junction potential was not corrected.

Stimulus protocols

Basal membrane properties

To measure basal membrane properties, 40 repetitions of a 200 ms current pulse of -5 pA were applied to patched neurons at resting membrane potential (RMP) with no holding current. The mean resulting potential drop was used to calculate input resistance (R_{in}), membrane capacitance (R_{in}) and the time constant tau (R_{in}). Only cells which reached a stable equilibrium potential within the 200ms stimulus were used for calculations.

Rheobase and current-frequency curves

To compare maximum firing frequencies of rattle and locomotor neurons and to measure rheobase currents, square current pulses of 1000 ms length and consecutively increasing amplitude were applied. To record current-frequency (I-F) curves, the amplitude of applied current-steps was increased in 25 pA steps, starting with a -50 pA stimulus current. For rheobase estimation, the same protocol was used. However, current amplitude was increased by 1 pA between individual current steps, starting with a stimulus amplitude estimated to lie slightly below rheobase.

Action potential properties

To measure the properties of individually elicited action potentials (APs), ramp stimuli with a rise time of $180 \mu s$ and a decay time of 1 ms were applied to mimic excitatory postsynaptic currents (EPSCs). The amplitude of the applied stimulus was increased in 100 pA steps. AP-analysis was performed after subtracting the last sub-threshold recording from the first supra-threshold recording, to adjust for sub-threshold potential-changes and allow for a direct measurement of only the AP defining parameters. Measurements

Please cite this article in press as: Bothe et al., Timing and precision of rattlesnake spinal motoneurons are determined by the KV7_{2/3} potassium channel, Current Biology (2023), https://doi.org/10.1016/j.cub.2023.11.062





included the amplitude of the AP and the after-hyperpolarization (AHP), as well as the full width at half maximum (FWHM) of AP and AHP.

Action potential firing precision

To measure the precision of motoneuron firing in the locomotor and rattle spinal cord regions, we applied ten or twenty repetitions of 1000 ms current pulses at rheobase. The mean and standard deviation of spike occurrence/latency was calculated as a measure for the "jitter" in a neuron's response. To quantify and visualize differences in the sub-threshold voltage responses of MNs, the integral between recording traces and a fictive horizontal line at the height of the new equilibrium potential was calculated for non-spiking repetitions

Pharmacology

To electrophysiologically evaluate the contribution of potassium channels on MN activity, α -dendrotoxin (100 nM), retigabine (10 μ M) and XE991 (15-20 μ M) were applied to the recording solution. Recordings were started 20 minutes after application of the respective drug. Shifts in resting membrane potential were compensated to pre-drug levels via current injection. During pharmacological treatment, we additionally applied synaptic blockers to reduce spontaneous synaptic input to the patched MNs (in μ M: DNQX: 20, strychnine: 0.5, D-AP5: 50, gabazine: 10).

Single cell RNA sequencing

51 locomotor MNs and 62 rattle MNs were individually collected from spinal cord slices of 6 rattlesnakes, transferred into 96 well plates containing lysis buffer and barcoded oligo-dt primers and stored at -80 until library preparation. Single-cell RNAseq libraries were prepared following the mcSCRB-seq protocol v 1.1. ¹⁰⁸ i7 index N714 was used for the locomotor cell plate, i7 index N715 was used for the rattle cell plate. Resultant libraries were then pooled and run on 0.5 lanes of a v4 high output flowcell, using an Illumina HiSeq 4000 sequencing instrument.

Bulk RNA sequencing

Tissues were dissected from rostral (RSC), medial (MSC) (i.e. locomotor), and caudal (CSC, i.e. rattle) spinal cord from three individual $Crotalus\ atrox$. RNA was isolated from tissues using a Qiagen RNEasy Mini Kit following manufactuer's instructions. Isolated total RNA was submitted to MSU RTSF Genomics Core, where sequencing libraries were prepared using Illumina TruSeq Stranded mRNA Library Preparation Kit. Libraries were quality controlled and quantitated using a combination of Qubit dsDNA assay, Caliper LabChipGX and Kapa Illumina Library Quantification qPCR kits. The libraries within each project were pooled for multiplexed sequencing. Each pool was loaded on one lane of an Illumina HiSeq 2500 Rapid Run (v2) flow cell to target \sim 15million paired reads per sample. To reach this target, additional sequencing was performed on a MiSeq using the same read format, and results were pooled.

Whole cord qPCR

RNA was isolated from snake spinal cord tissue using a spin-column system (ROTI®Prep RNA MINI kit, Carlroth GmbH + Co. KG, 76185 Karlsruhe, Germany) and followed the standard protocol supplied with the kit. In brief, segments from locomotor (n=8 specimens from N=6 animals) and rattle spinal cord (n=8 specimen from N=6 animals), weighting between 5 and 19 mg were dissected on ice and immediately transferred to lysis buffer. The tissue was homogenized (Qiagen Tissue Lyser II) and unlysed material was precipitated by centrifugation. In a next step, DNA was removed by centrifugation through a DNA-binding spin-column. Afterwards, RNA was bound by another centrifugation step through a RNA binding spin column. After several washing steps, RNA was eluted in RNase free water and the total RNA concentration in the eluate was quantified (NanoDrop One Microvolume UV-Vis Spectrometer, Thermo Scientific, Waltham, MA02451, United States). Samples were stored at -80°C until further use.

For qPCR, 100 ng of total RNA were used for cDNA synthesis and subsequent multiplex PCR assays. cDNA synthesis and qPCR were performed using a real-time PCR detection system (CFX 96 Touch, Biorad, Hercules, California, United States) and followed standard protocols provided by the supplier (Biorad, iScript™ cDNA Synthesis Kit and PrimePCR Assay using the iQ™ Multiplex Powermix). In brief, after cDNA synthesis in a thermal cycler (20min at 46°C, 1min at 95°C, hold at 4°C), multiplex qPCR was performed. A mastermix was prepared that included fluorophore-tagged primers specific for the target DNA (Table S4) and the necessary reaction mix. Equal amounts of cDNA were added from each spinal cord RNA sample and real-time qPCR of individual samples (loco, n=8; rattle, n=8) was performed in a thermal cycler (2 min at 95°C, 40 cycles of 95°C for 10 s and 60°C for 45 s, hold at 4°C). Expression in locomotor specimen was used as the control against which differential expression in rattle specimen was tested, using ΔΔCq analysis.

QUANTIFICATION AND STATISTICAL ANALYSIS

If not stated otherwise, all values are given as mean \pm S.E.M. In boxplots, the central marker (line) indicates the median value and the bottom and top edges of the box show the 25th and 75th percentiles, respectively.

In-vitro slice physiology

For patch clamp experiments, significance of differences was tested using either the non-parametric Wilcoxon signed-rank test for paired data (pharmacology), or the non-parametric Mann-Whitney-U test for unpaired data. In boxplots, the central marker (line)

Please cite this article in press as: Bothe et al., Timing and precision of rattlesnake spinal motoneurons are determined by the KV72/3 potassium channel, Current Biology (2023), https://doi.org/10.1016/j.cub.2023.11.062

Current Biology Article



indicates the median value and the bottom and top edges of the box show the 25th and 75th percentiles, respectively. Exact numbers of cells analyzed in each experiment are given in the respective sections of the main text.

Single cell RNA sequencing

Raw single cell sequencing data was processed using the zUMIs pipeline, 113 which filters reads with low-quality barcodes and UMIs, and then uses the STAR aligner v2.7.3a¹¹⁴ to align reads to the Crotalus tigris genome (NCBI RefSeg GCF_016545835.1).¹¹⁵ zUMIs then predicts cell barcodes and collapses UMIs to create a read count table for downstream analysis. We retained barcodes (putative cells) that had between 10,000 and 125,000 mapped reads and then 3000 uniquely mapped features (genes), leaving a final analysis set of n=41 rattle MNs and n=34 locomotor neurons. Next, we generated read count tables and analyzed them using the Seurat R package. 116 We used the Seurat "FindMarkers" function to conduct a Wilcoxon Rank Sum test to determine differentially expressed genes between the locomotor and rattle MN pools. All code for data analysis can be found at zenodo (see key resources table).

Bulk RNA sequencing

Raw bulk sequencing data was trimmed for adapter sequences and low-quality sequences using Trimmomatic v0.38¹¹⁷ with the following parameters LEADING: 5 TRAILING: 5 SLIDINGWINDOW: 4:5 MINLEN: 25. Next, RSEM v1.3.3¹¹⁸ was used with the STAR aligner v2.7.3a¹¹⁴ to align reads to predicted transcripts from the Crotalus tigris genome (NCBI RefSeq GCF_016545835.1). 115 Uniquely mapped reads from our samples ranged from 75-79%. RSEM counts were then imported into R using tximport v.1.26.0¹¹⁹ and differential expression was analyzed using DESeq2 v1.38.1.¹²⁰ Differential expression analysis was performed by comparing expression in the caudal spinal cord ("CSC", i.e. rattle) to the combined rostral and medial spinal cord ("RSC+MSC", i.e. locomotor) samples using a log-ratio test (LRT). P-values were adjusted for multiple comparisons using the Benjamini and Hochberg method, ¹²¹ with a false discovery rate (FDR) threshold of 0.1. All code for data analysis can be found at zenodo (see key resources table).

Whole cord qPCR

Significance of expression differences in qPCR experiments was tested using analysis of variance (ANOVA), applied by commercially available software (CFX Maestro, Biorad, Hercules, California, United States).